Advanced Composites and Hybrid Materials (2024) 7:114
https://doi.org/10.1007/s42114-024-00930-6

REVIEW

Progress of MOFs and their derivatives for mitigating air pollution

Xiaoyi Duan[1] · Xiangmeng Chen[1] · Cheng Li[1] · Erin Witherspoon[2] · Ethan Burcar[2] · Zhe Wang[2] · Wanxi Peng[1] · Aricson Pereira[3] · Hanyin Li[1]

Received: 20 February 2024 / Revised: 27 May 2024 / Accepted: 22 June 2024 / Published online: 2 July 2024

Abstract

The post-industrial revolution era has witnessed unprecedented economic and technological growth, leading to a significant surge in population and industrial advancements. However, this rapid progress has been accompanied by a concerning increase in environmental degradation, resulting in mass extinctions and posing a serious threat to both ecosystems and human health. Addressing these pressing challenges requires innovative solutions. Metal-organic frameworks (MOFs), which are crystalline structures made of metal ions or clusters interwoven with organic ligands, are one intriguing technique. MOFs have gotten a lot of interest because of their amazing specific surface area, tunable pore size, and adaptability. Their development holds significant potential for mitigating industrial waste gas emissions and improving environmental quality across various applications. This comprehensive review delves into the pivotal role of MOFs in air purification. Beginning with an exploration of the hazards, origins, and complexities of haze, the review meticulously examines the applications of MOFs in addressing various pollutants, including SO_2, NO_x, $PM_{2.5}$, automobile exhaust, coal-fired flue gas, fuel emissions, and incineration byproducts. Each section provides insight into design principles, adsorption mechanisms, and transformation processes for effective pollutant mitigation. Overall, this review demonstrates an array of effective and environmentally sound technical methodologies, underscoring the pivotal role of MOFs in combating multifaceted air pollution. It serves as a valuable resource for researchers and practitioners seeking sustainable solutions to complex environmental challenges.

Keywords MOFs · Purification and separation · Pollutant gases · Improve air quality

1 Introduction

1.1 The harm of haze

Although the overconsumption of natural resources has contributed to industrialization and economic development, resulting in significant material progress, the environmental costs have been high, especially in terms of atmospheric changes, which have caused serious problems [1]. The use of fossil fuels like coal and oil has led to the regular occurrence of smog events that draw attention from all around the world [2]. Haze pollution is characterized by fine particulates matter and reduced visibility to less than 10 km. The impact of smog pollution has far-reaching implications, including adverse effects on traffic [3, 4], human health [5] (Table 1), infant stunting [23], and environmental quality [24]. Research has indicated a clear correlation between air pollution and the quality of human life [25–28].

The issue of smog can be traced back to the industrialization of developed nations like the United Kingdom and the

Xiaoyi Duan, Xiangmeng Chen, and Cheng Li, who were co-first authors, contributed equally to this work.

✉ Xiangmeng Chen
xmchen0610@163.com

✉ Wanxi Peng
pengwanxi@163.com

✉ Hanyin Li
lihanyin@henau.edu.cn

[1] School of Forestry, Henan Agricultural University, Zhengzhou 450002, China

[2] Department of Chemistry, Oakland University, Rochester, MI 48309, USA

[3] Advanced Materials Division, Engineered Multifunctional Composites (EMC) Nanotech LLC, Knoxville, TN 37996, USA

Table 1 Effects of air pollution on human health

System	Impacts on health	Air pollutants	References
Respiratory	Respiratory emergency hospital visits	$PM_{2.5}$, PM_{10}, NO_2, SO_2	[6]
Respiratory	Child lung function	PAHs, benzene, toluene, ethylbenzene, 1,2-dimethylbenzene	[7]
Circulatory	Hypertension	$PM_{2.5}$	[8]
Circulatory	Circulatory emergency department visits	SO_2	[9]
Circulatory	Cardiovascular, ischemic heart disease and high blood pressure emergency department visits	$PM_{2.5}$	[10]
Circulatory	Type II diabetes mellitus hospitalization	$PM_{2.5}$, PM_{10}, NO_2, SO_2, CO	[11]
Digestive	Peptic ulcer bleeding	NO_2	[12]
Digestive	Hand-foot-and-mouth disease	SO_2	[13]
Nervous	Insomnia	AQI, $PM_{2.5}$	[14]
Nervous	Daily admissions for mental disorders	PM_{10}, SO_2, CO	[15]
Nervous	Hospital admissions for overall and specific mental disorders	$PM_{2.5}$, PM_{10}, PM_C	[16]
Nervous	Hospital visits for ye and adnexa diseases	NO_2	[17]
Urinary	Kidney function	Individual average daily dose	[18]
Urinary	Chronic kidney disease	NO_2, $PM_{2.5}$, $PM_{2.5\text{-}10}$, PM_{10}	[19]
Pregnancy	Likelihood of female offspring	PM_{10}, SO_2, NO_2	[20]
Pregnancy	Preterm birth	PM_{10}, O_3	[21]
Pregnancy	Fetal distress	$PM_{2.5}$	[22]

USA [29]. In a study by Leleveld et al. [30], global satellite observations, ground-based observations, and atmospheric chemistry models were employed to analyze the impact of worldwide atmospheric pollution sources on premature mortality. It was discovered that the usage of solid fuels for cooking and heating results in indoor air pollution, which claims the lives of almost 3.54 million people per year. The primary cause of death in China is air pollution, which causes more deaths than traffic accidents and HIV combined. In Southeast Asia, India has the highest mortality rate, with 650,000 premature deaths yearly.

1.2 Causes of haze

Atmospheric visibility is intrinsically linked to $PM_{2.5}$ particle concentration in the air. Smog, a phenomenon that results in impaired visibility, is primarily caused by sulfates, ammonium, and nitrates carried by $PM_{2.5}$ particles. Both natural and man-made processes, such as the burning of fossil fuels or biomass, industrial processes, and automobile emissions, can produce these particles. With a cycle ranging from days to weeks, $PM_{2.5}$ particles can travel thousands of kilometers, making them a significant contributor to haze formation. The small size of $PM_{2.5}$ particles enables them to scatter light efficiently, which significantly impacts visibility. The photochemical oxidation of volatile organic compounds (VOCs) in metropolitan settings, where emissions of VOCs from biogenic and anthropogenic sources are large, produces various semi-volatile and non-volatile chemicals that are essential to the conversion process of gas into particles. The vapor phase oxidation of volatile organic molecules by free radicals such as OH, NO_3, or ozone further exacerbates the issue.

During the daytime, the oxidation of VOCs induced by hydroxyl radicals (OH) results in the formation of various organic products with oxygen-containing functional groups. These products include aldehydes, ketones, alcohols, carboxylic acids, hydrogen peroxide, percarboxylic acids, and peroxyacylnitrates [31]. The initial oxidation step generates some compounds that undergo subsequent oxidation processes. This leads to multigenerational products with lower volatility and higher solubility than the parent chemical. In urban environments, aromatics such as toluene, xylene, and trimethylbenzene account for a substantial portion (over 20%) of all volatile organic chemicals [32, 33]. Human activities are the primary cause of aromatic hydrocarbon emissions, particularly from automobiles, fuel-powered vehicles, and industries. Toluene concentration in urban areas may range from 1 to 200 pounds, depending on the source and location of emissions [32–34]. Aromatic hydrocarbons typically have a short lifespan of 0.5 day to 2.5 days and are not reactive with OH free radicals. However, when OH aromatic reaction occurs, it can produce two types of chemicals: ring-opening chemicals such as glyoxal and methyl glyoxal, and ring-preserving chemicals such as benzaldehyde and cresol [35]. Regardless of the initial toluene level, it has been noted that under low nitrogen oxides (NO_x), circumstances, the oxidation product of toluene-OH on

pre-existing ammonium sulfate aerosol produces 30% of the secondary organic aerosol. Aromatic oxidation also affects black carbon (BC) particles, altering their composition and increasing their density, hygroscopicity, and optical qualities.

1.3 Application of metal-organic framework and their derivatives in air pollution control

Air pollution levels vary across regions and cities due to differences in natural and climatic conditions, topography, air pollution sources, and energy consumption. While national policies play a significant role, local measures need to be implemented to address specific air pollutants [36, 37]. Sustainable development in the environment includes the protection of biodiversity and the reduction of atmospheric $C0_2$ concentrations and pollutants [38]. Despite numerous studies on catalysts since the 1990s, removing haze under lean operating conditions remains a significant challenge. In China, studies have been conducted to enhance high velocity catalytic activity [39, 40]. In the realm of environmental catalysis, the removal of methane from compressed natural gas vehicle exhaust is a significant challenge due to its resistance to conventional three-way catalysts. Metal-organic framework (MOF) possess a highly porous structure and an enormous specific surface area, enabling them to effectively adsorb various air pollutants, including fine particulate matter ($PM_{2.5}$ and PM_{10}), VOCs, NO_x, and sulfur dioxide (SO_2). The pore size of MOFs can be controlled by selecting different organic ligands, allowing them to adsorb pollutants of different sizes. Due to their structural stability, MOFs can maintain excellent adsorption performance under harsh environmental conditions, making them suitable for use as catalysts for automotive exhaust purification, converting harmful gases into harmless substances. This property is particularly well-suited for industrial waste gas and exhaust purification applications. Furthermore, due to the diverse composition and tunable structure of MOFs, they are considered suitable precursors for the preparation of porous materials. They are typically prepared through thermal decomposition or solution infiltration under specific conditions. By precisely controlling the precursor and synthesis process of MOFs, it is possible to prepare derivative materials with more diverse pore sizes, appearances, compositions, and properties than the precursor material itself. The main methods for preparing these derivative materials include direct thermal decomposition of MOFs [41], co-thermal decomposition with other precursors [42], and thermal decomposition of composite materials [43], as well as solution infiltration followed by heat treatment [44]. Researchers interest in MOFs materials has grown due to their potential to help with air purification and pollution management in this setting (Table 2).

2 Adsorption and conversion of sulfur dioxide using MOFs

Sulfur dioxide is a prevalent industrial exhaust gas that threatens both the environment and human health. Scientists have made significant progress in developing a range of MOFs adsorbents, including MOF-74, MFM-300, MFM-601, MOF-160, Ni8(L)6, and UiO-66, which can effectively adsorb and convert sulfur dioxide. These MOFs materials exhibit automatic air purification and separation, allowing them to treat various harmful gases and exhaust emissions. The continued development of MOF materials is essential to reducing industrial exhaust emissions and enhancing environmental quality. It is imperative to note that air pollution can have a profound impact on the Earth natural cycles, particularly the sulfur cycle [31]. The atmosphere is naturally exposed to sulfur dioxide through various sources such as volcanic eruptions, spring water, air currents, organic decomposition, and anaerobic bacteria. However, significant quantities of this gas are released into the atmosphere through human activities such as fossil fuel burning, food production, transportation, and activities in the oil industry. The increasing levels of sulfur dioxide in the atmosphere have resulted in severe damage to ecosystems and loss of biodiversity, and pose a significant threat to human health. Inhalation of sulfur dioxide through the lungs and skin can result in respiratory illnesses and fatalities, especially when concentrations reach up to 100 ppm [82]. Once released into the atmosphere, SO_2 readily dissolves in water to form sulfuric acid (H_2SO_4) in contact with oxygen. These acids cause soil and water pollution through wet sedimentation, affecting the growth of forests and crops. In most urban areas, the formation of $PM_{2.5}$ is associated with SO_2.

2.1 MOFs design for SO_2 adsorption

MOFs are a family of crystal materials made up of organic ligands and metal ions or clusters. These structures have a large surface area, adjustable pore sizes, and remarkable flexibility in terms of absorbing, holding, and adsorbing materials. Construction of MOFs involves the use of organic linkages such as carboxylic acids or azo ligands [84], as well as metal ions or clusters [85]. With varying properties of ligands and metal centers, these materials form one-, two-, or three-dimensional arrays. The versatility of MOFs allows them to exhibit various properties such as capture, repair, catalysis, chemical sensing, gas separation, and storage. Furthermore, MOFs can be easily prepared with different chemical compositions and ligand functions, at a lower cost than traditional porous materials, stimulating a growing interest in its application [86].

Table 2 Separation of atmospheric pollutants by MOF catalysts

Pollutant	Kinetic diameter	MOFs	Efficiency (%)	Ref.
SO_2	0.28/nm	MOF-74	100	[45]
SO_2	0.28/nm	MFM-300	ND	[46]
SO_2	0.28/nm	MFM-601	ND	[47]
SO_2	0.28/nm	NH2-UiO-66	ND	[48]
SO_2	0.28/nm	MOF-177	ND	[49]
SO_2	0.28/nm	NH2-MIL-125 (Ti)	ND	[50]
SO_2	0.28/nm	MIL-160	ND	[51]
NO_2	0.3675/nm	UiO-66	73	[52]
NO_2	0.3675/nm	UiO-67	79	[52]
NO_2	0.3675/nm	HKUST-1	ND	[53]
NO_2	0.3675/nm	Mg-MOF-74	40	[54]
NO_2	0.3675/nm	Fe-MOF-5	95	[55]
NO_2	0.3675/nm	$[Zr_6O_4(OH)_4(FA)_6]_2(cal)_3$	ND	[56]
NO_2	0.3675/nm	MFM-300(Al)	ND	[57]
Germs	ND	BIT-66	99.6	[58]
Germs	ND	ZIF-8	96	[59]
Germs	ND	MOF-53(Fe)@Van	> 99.9	[60]
Germs	ND	E-MOFilter	99.3	[61]
Microplastics	1 μm–5 mm	MIL-100	90	[62]
Microplastics	1 μm–5 mm	MIL-101	ND	[63]
Microplastics	1 μm–5 mm	UiO-66	ND	[64]
Microplastics	1 μm–5 mm	ZIF-67	72.7	[65]
Microplastics	1 μm–5 mm	ZIF-8	92.1	[66]
Microplastics	1 μm–5 mm	UiO-68	99	[67]
Microplastics	1 μm–5 mm	PTZ-1	ND	[68]
$PM_{2.5}$	≤2.5 μm	Ag-MOFs@CNF@ZIF-8	ND	[67]
$PM_{2.5}$	≤2.5 μm	TiO_2@NH_2-MIL-125	ND	[69]
$PM_{2.5}$	≤2.5 μm	TiO_2-UiO-66-NH_2	ND	[70]
$PM_{2.5}$	≤2.5 μm	TiO_2	ND	[71]
NO	ND	TiO_2	ND	[72]
NO_X	ND	TiO_2	ND	[73]
TCE	ND	TiO_2	ND	[74]
CH4	0.38/nm	MOF-177	ND	[75]
CO_2	0.33/nm	MIL-160	ND	[51]
CO_2	0.33/nm	NH2-MIL-101	79.4	[76]
CO_2	0.33/nm	Mg-MOF-74	100	[77]
CO_2	0.33/nm	UiO-68-NHC	> 90	[78]
NH_3	0.365-0.38/nm	M-CPO-27	ND	[79]
H_2S	ND	MIL-53(Cr, Al, Fe)	ND	[80]
C_2H_4	ND	MOF-199	ND	[81]

Note: *ND*, no available data

MOFs possess the unique ability to accommodate inorganic clusters including Keggin anions and metal nanoparticles. Catalytic sites can be added to the organic support that spans the metal nodes, or catalytic metal elements can be used to modify the organic connections. It is possible to customize the metal center in the MOFs to evoke desired functions by adjusting the stereoelectronic features of the connection. Zeolites, with their exceptional cation exchangeability, facilitate the preparation of metal nanoclusters, resulting in the uniform dispersion of electrostatically driven cation precursors. Furthermore, the high thermal stability of zeolites promotes the proper conversion of precursors, such as decomposition or calcination of organometallics. The various coupling of internal or exterior catalytic metal clusters with Brønsted or Lewis acid sites in zeolite materials has enabled numerous applications of

these materials as metals [87]. Conventional desulfurization techniques such as limestone cleaning are effective in removing a significant proportion of SO_2 from exhaust gases. However, residual SO_2 can still have adverse effects on both the environment and human health [88]. Capturing the tiny quantities of SO_2 found in exhaust gases so becomes crucial. The creation of a strong and potentially irreversible metal-sulfur connection has made it difficult to use metals to capture this undesirable SO_2. This bond has the potential to disrupt other coordination contacts between the metal center and the ligand, resulting in structural collapse.

2.2 Adsorption and transformation mechanism of SO_2

Using one-dimensional [AlO4(OH)2] chains and biphenyl 3,3′, 5,5′-tetracarboxylate, NOTT-300 [46], also known as MFM-300 (Al) (Fig. 1), was produced. It has been

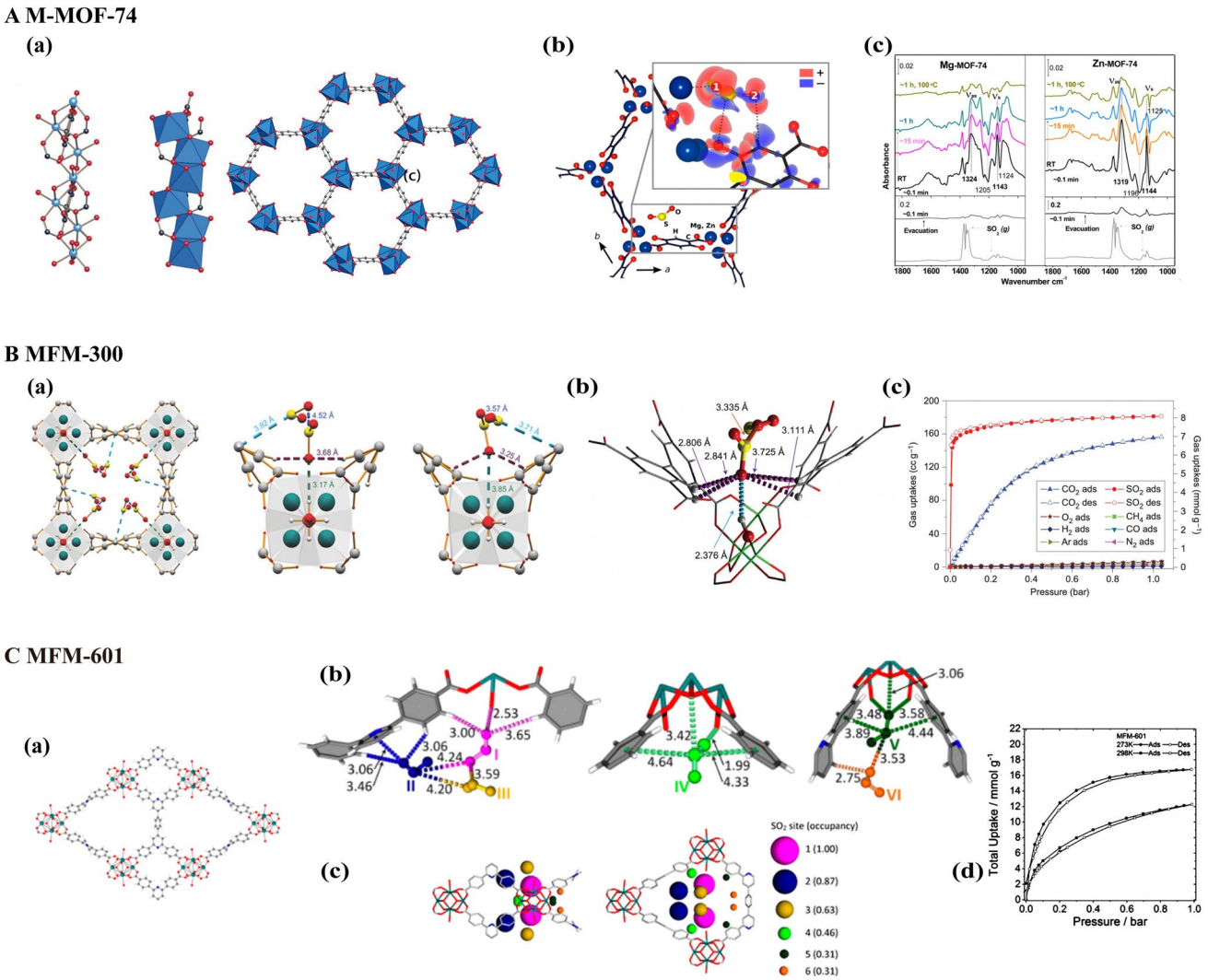

Fig. 1 **A** M-MOF-74. **a** Structure of M-MOF-74. Reprinted with permission from [89], Copyright 2005, American Chemical Society. **b** M-MOF-74 in contact with SO_2 (M = Mg, Zn). Reprinted with permission from [45], Copyright 2017, American Chemical Society. **c** The charge density varies with the increase of adsorption area. Blue represents Mg or Zn; red represents oxygen; black represents carbon; white represents hydrogen; and yellow represents sulfur. Reprinted with permission from [45], Copyright 2017, American Chemical Society.; **B** MFM-300. **a** structure of 300 and SO_2 molecules adsorbed in MFM-300 (In). Reprinted with permission from [90], Copyright 2020, American Chemical Society. **b** The main internal interaction of MFM-300-SO_2 Reprinted with permission from [46], Copyright 2012. **c** Isotherms of MFM-300 (Al) for adsorption of different gases. Reprinted with permission from [46], Copyright 2012; **C** MFM-601. **a** structure of MFM-601. Reprinted with permission from [47], Copyright 2018, Joseph H. Carter. **b** SO_2 binding sites in MFM-601. Reprinted with permission from [47], Copyright 2018, Joseph H. Carter. **c** The occupancy rate of SO_2 in MFM-601. Reprinted with permission from [47], Copyright 2018, Joseph H. Carter. **d** SO_2 adsorption isotherms of MFM-601. Adapted with permission from [47], Copyright 2018, Joseph H. Carter

demonstrated that SO_2 molecules and hydroxyl groups on Al SBU form hydrogen bonds. There is also a mild synergistic effect between neighboring C-H groups on the ligand benzene ring and SO_2 molecules. Furthermore, Marilyn and his colleagues [48] modified UIO-66 with alkaline groups such as $-NH_2$ in order to enhance the ability of MOFs to respond to acidic gases such as SO_2, NO_2, and CO_2. The findings suggest that the electronic properties of the MOF are altered by the interaction of these gases with the $-NH_2$ groups on the linker [90].

The interaction between SO_2 molecules and the host skeleton can significantly impact MOF changes [90]. Mechanism investigations have revealed that strong contact between SO_2 and hydroxyl groups increases molecular interactions during the adsorption process, leading to an increase in SO_2 dipole moment. It was reported that MFM-601 (Fig. 1), based on Zr, exhibits excellent SO_2 adsorption performance [47]. By leveraging the dipole moment of SO_2, MFM-601 provides stable binding in the pore in addition to promoting the interaction between SO_2 molecules. Strong adsorption sites are provided by the MOFs nodes, and to improve SO_2 molecule capture, metal cations can be post-modified and added to the porous core material. Furthermore, the addition of Ba^{2+} to the defect site of nickel pyrazolate-based MOFs can also enhance their interaction with SO_2.

2.3 MOFs preparation for adsorption and conversion of SO_2

MOFs contain highly active metals that interact with sulfur dioxide (SO_2) to form Lewis acid, which aids in adsorption. Sun et al. [91] examined the adsorption characteristics of 12 distinct porous materials, such as MOF, zeolite, and ZIF, using molecular simulations, or Grand Canonical Monte Carlo. They discovered that because of the high density of exposed metal components in the framework, Mg-MOF-74 can remove CO_2, SO_2, and NO_x from the environment all at once. Moreover, Chabal et al. [45] used DFT analysis and in situ infrared spectroscopy to examine the relationship between SO_2, NO_2, and M-MOF-74 series metal frameworks. A case in point is the MOF-74 structure with zinc open metal sites as depicted in Fig. 1. Glover [80] conducted a study on various metals (M=Co, Mg, Ni, Zn) within the MOF-74 series, demonstrating the dynamic breakthrough capacity for removing hazardous gases including SO_2, from the air under dry and wet conditions. The findings indicate that the simulated Mg-MOF-74 material has an excellent adsorption effect on SO_2. However, due to competition between water and SO_2 molecules at open metal sites, the gas adsorption capacity is reduced in high humidity conditions. Water molecule adsorption often reduces M-MOF-74 ability to effectively absorb visitor molecules. In a separate research, due to water being the most common impurity in organic solvents, it often affects the yield and activity of products in many organic synthesis reactions and industrial processes. Guo et al. [92] utilized a solvothermal method to synthesize a smart fluorescent pyrene-based MOF (HPU-26), which can self-decompose and release ligands under the driving force of water molecules. The MOF exhibits multi-stimulus responsive properties, changing its fluorescent color from yellow-green to blue, making it easily visualized, and enabling detection of water content in common organic solvents.

NOTT-300 is comprised of MOF materials functionalized with OH hydroxyls. The MOF has an angular-extended octahedral chain composed of $[AlO_4(OH)_2]$ linked by an H_4L ligand (bipheny-3,3′, 5,5′-tetracarboxylic acid). This frame structure has a diameter of 6.5 and features a 6.5 Å square channel with a free (cis-OH) hydroxyl group. MFM-300 (Al) (Fig. 1) exhibits remarkable selectivity in adsorbing CO_2 and SO_2 between 273 K and 303 K. At 273 K and 1 bar, a fully reversible desorption isotherm was reported, with a maximum adsorption of 7.0 mmol g^{-1} for CO_2 and 8.1 mmol g^{-1} for SO_2. Furthermore, the SO_2 isotherm indicates that SO_2 adsorption is maximized at extremely low pressures due to the strong contact between MFM-300 (Al) and SO_2, which is caused by the large dipole moment of SO_2. The -OH hydroxyl group of the MFM-300 (Al) skeleton is the main binding site for SO_2, according to Rietveld refinement by X-ray powder diffraction. Together with four weaker C-H-O=S=O hydrogen bonds, this group also produces strong Al-OH-O=S=O hydrogen bonds with nearby hydrogen atoms. O=S · · O=S=O is used by the second SO_2 molecule to create an intermolecular chain with the first SO_2 molecule when it enters the solution. Due to its high capture capacity under low pressure, MFM-300 is a promising candidate for SO_2 capture. Eddaoudi and Salama [93] found that the high SO_2 adsorption capacity of MFM-300 makes it ideal for SO_2 sensors. The capacity of this material to remove sulfur dioxide from flue gas selectively is confirmed by the fact that these sensors can efficiently collect sulfur dioxide even under actual flue gas settings.

3 Adsorption and conversion of nitrogen oxides using MOFs

Since the onset of the industrial revolution, fossil fuel extraction, production, and consumption have steadily increased. Unfortunately, this has led to the release of an ever-increasing number of harmful chemicals such as nitrogen oxides (NO_x) into the atmosphere. The environment and public health are seriously threatened by the emission of these pollutants. Thus, it is essential to provide hazardous gas control and treatment a lot of attention [90]. Among the nitrogen oxide family, nitrogen dioxide is more toxic than nitric

oxide. Nitrogen dioxide is highly corrosive and can damage materials irreparably. In the past, traditional "capture" techniques for nitrogen oxides, including selective catalytic reduction [94], activated carbon adsorption, and zeolite, have been employed. However, the reduction of NO_2 to NO during carbon surface oxidation is an inevitable outcome of all these techniques [95]. As a result, researchers have studied various strategies for reducing NO_2 to NO, hoping to overcome this significant challenge. Han et al. [96]. used a MOF with variable valence vanadium metal centers, MFM-300 (VIII, IV), to adsorb and reduce nitrogen dioxide (NO_2), and revealed the interaction between NO_2 molecules and the active MOF through in situ X-ray diffraction technology. The vanadium metal center in the MOF has REDOX activity. The nitrogen dioxide is absorbed in MFM-300 (VIII) pore and reduced to NO at the same time, and the vanadium metal center of MOF is oxidized from trivalent to quadrivalent. Molecularly porous materials, or MOFs, have emerged as a promising field of research in gas separation and have received considerable attention from researchers.

3.1 MOFs design principle for NOx adsorption

MOFs are renowned for their enormous specific surface area, porosity, and adaptable topological structure to various demands. Different metal and organic ligands are used in the MOFs synthesis process, which can produce alkaline or acidic crystalline porous MOFs networks. This chemical diversity makes it possible to customize MOFs composition according to their specific needs. MOFs central cavities with varying shapes can be obtained using the same ligand and resulting in a variety of porosities in the final product. This high porosity is comparable to activated carbon and is an advantage over traditional porous materials like zeolite. Because MOFs have a high-specific surface area and porosity, they are perfect for a variety of uses.

Because of their special qualities, MOFs have emerged as viable options for the adsorption of dangerous gases. The adsorption capacity of graphite oxide composite materials and HKUST-1 for ammonia was examined in a recent research [97]. HKUST-1 has shown to be an effective adsorbent for H_2S and NO_2 [98], but the structural integrity of the framework is compromised during the adsorption process, rendering it unusable for further use. MOFs with different ligands exhibit distinct structural properties and, therefore, varying adsorption abilities. Research has been conducted to explore the effect of different oxidized foreign metals introduced into MOFs on gas adsorption [99]. The doping of metal ions can provide additional adsorption sites and improve efficiency. A study conducted by Amani et al. [52] involved the addition of Ce^{3+} to MOFs and doping Ce^{3+} with Zr-based MOFs as a NO_2 adsorbent. The surface chemistry, structural characteristics, and adsorption performance of the material were analyzed. It was discovered that oxidation-reduction events occurred and the number of active sites increased, indicating that metal doping is advantageous for NO_2 adsorption.

3.2 Adsorption and transformation mechanism

Research shows that the porosity, stability, and corrosion resistance of NO_2 can be improved using metal-doped MOFs. When the number of carboxylic acid reaction ligands is restricted as in the case of benzenediazonium chloride, a mixed Ce-Zr-MOF phase is formed. The Ce^{3+} interacts with carboxyl groups, thereby limiting the amount of space available for water and adsorbent molecules to enter the pores. The increase in NO_2 adsorption is attributed to redox oxidation. The crystal surface structural properties regulate the development of new micropores in Ce doping which in turn increases NO_2 adsorption [52].

The capability of Cu-based skeleton HKUST-1 for NO_2 adsorption is demonstrated in Fig. 2. The graphite oxide composite material GO-HKUST-1 of HKUST-1 exhibits a range of 2.43–2.91 mmol/g for dry NO_2 adsorption and 0.83–1.28 mmol/g for 70% humidity-induced NO_2 adsorption [102]. It is noteworthy that the BET surface areas of both HKUST-1 and GO-HKUST-1 witnessed a significant reduction of 90% and 80%, respectively. Findings from differential thermogravimetric analysis and infrared spectroscopy analysis indicated that MOF degradation occurred due to the reaction between Cu nodes and NO_2, leading to the formation of bidentate nitrates [52].

The study of UiO-66-NH_2 has allowed for more research on the modification of UiO-66 by linkers. NO_2 was discovered to have an adsorption capacity of 20.3 mmol/g when it was dry, but 31.2 mmol/g when it was found to be at 80% humidity [103], showing a considerable increase in the adsorption rate. Nuclear magnetic resonance, X-ray photoelectron spectroscopy, infrared, and other characterization methods were used to investigate the mechanism behind the adsorption of NO_2 by UiO-66-NH_2. These studies suggested that NH_2 groups facilitate the production of diazonium ions, which in turn react with NO_2. McGrath et al. have reported that aryl diazonium salts generate phenol while releasing N_2 gas to remove NO_2 [104]. The metal framework does not break down when bonds cleave, even if chemical processes do occur within it.

To create UiO-66-Ox, free carboxylic acid was added to UiO-66. The NO_2 capture capacity of UiO-66-Ox was found to be 8.4 mmol/g, which was much greater than that of UiO-66 through a microbreakthrough experiment [104]. The interaction between free COOH groups and NO_2, which raises gas adsorption rates, is responsible for this enhancement. However, the structure of UiO-66-O_x decomposes automatically after exposure to NO_2. Metal ions doping was

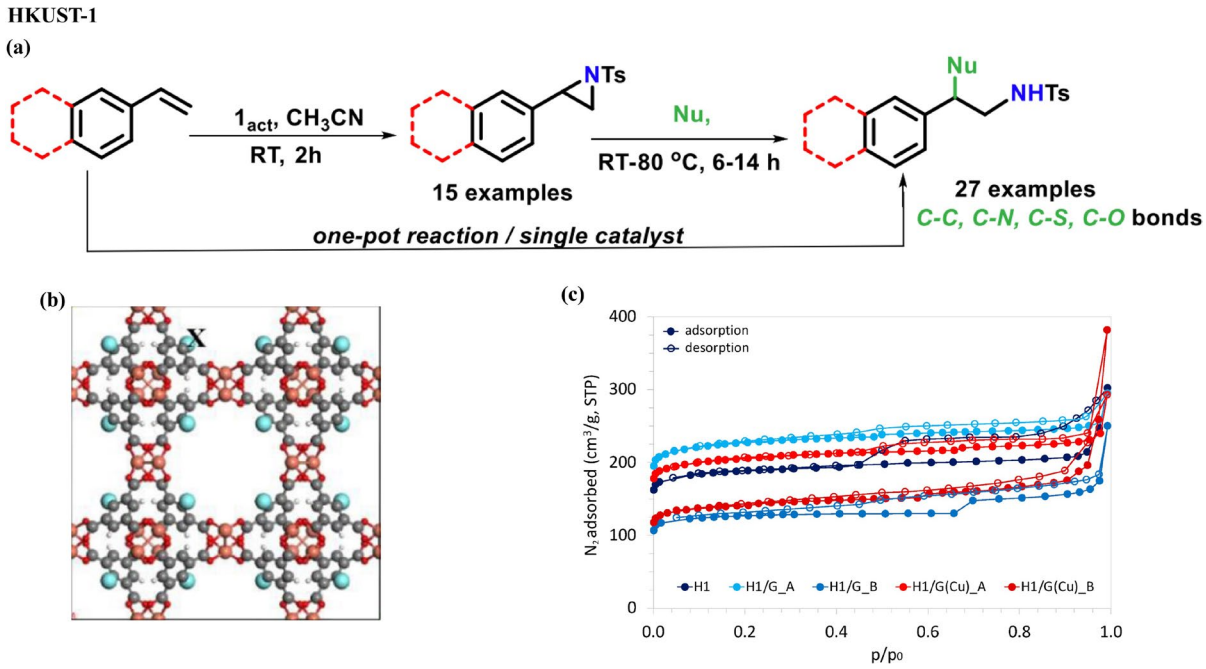

Fig. 2 HKUST-1: **a** MOF catalyzed one-pot synthesis of β-aryl sulfonamides derivative via olefin aziridination. Reprinted with permission from [53], Copyright 2021, Sajan Pradhan. **b** Unit cell of bulk structure. Reprinted with permission from [100], Copyright 2020, Royal Society of Chemistry. **c** Adsorption of N_2 in composite materials HKUST-1 and HKUST-1/GO at standard temperature and pressure; the filled sign denotes adsorption and the open symbol desorption. Reprinted with permission from [101], Copyright 2022, Paulina Jagódka

explored as an alternative to functionalize Zr-UiO-66 nodes and connections. UiO-66 and UiO-67 were doped with Ce^{3+} during the dry synthesis process. Greater NO_2 adsorption is achieved by the Ce-doped UiO-66 and UiO-67 structures because they have more adsorption sites. However, the structure stability of the Ce-doped framework deteriorated when exposed to NO_2 [52].

The Zr-based MOF $[Zr_6O_4(OH)_4(FA)_6]_2(cal)_3$ has been identified as a highly effective yet reversible NO_2 sensor. This is achieved through the use of calixarene as a linker and a unique charge transfer process between calixarene and NO_2 at ambient temperature [56]. The charge transfer is attributed to the creation of N_2O_4, which undergoes disproportionation into NO^+ and NO_3^-. The study identified that the development of purple charge transfer complexes occurs under the encapsulation of NO^+ molecules, along with the coordination of NO_3^- and Zr^{4+} sites, which was verified by UV-visible and infrared spectra. It was further observed that the MOF crystallinity remained unaltered even after repeated exposure to NO_2. Figure 2 illustrates that low NO_2 concentrations below 1 ppm have a major effect on elimination in addition to having an adsorption capacity of 14.1 mmol/g. The creation of one-dimensional helical chains of $(NO_2 \cdots N_2O_4) \infty$ monomer dimers in MFM 300 (Al) enhances the interaction between porous host molecules and guest molecules (Fig. 3). Furthermore, the stability of the MFM-300 (Al) structure is demonstrated by its ability to undergo five NO_2 adsorption and desorption cycles. Furthermore, studies show that copper-containing HKUST-1 can adsorb about 9 mmol g^{-1} of NO at 296 K, making it one of the most promising porous materials with remarkable adsorption ability [105]. The robust interaction between NO and Cu ions within the framework can be ascribed to this. Furthermore, researchers have explored selective Ni doping in the Mg-MOF-74 framework to improve adsorption. Mg-MOF-74 doped with 40% Ni^{2+} was found to demonstrate excellent NO adsorption and transport capability [54].

In a recent study, it was discovered that NO binds strongly to unsaturated redox-active Fe^{2+} in Fe-MOF-74, resulting in the formation of a Fe-NO adduct. The oxidation of the Fe^{2+} site was correlated with a distinct color change when exposed to NO. In addition, the study was extended to a different iron-ordered mesoporous siliceous framework where Fe^{2+} swaps MOF-5 (Fig. 3) and disproportionates NO to produce nitrite iron complexes and N_2O [55].

4 Adsorption and conversion of VOCs and $PM_{2.5}$ using MOFs

Urbanization and industrialization have contributed to the rise of air pollution, particularly in the form of $PM_{2.5}$ (pneumatic diameter 2.5 μm), which is dangerous for human health and daily activities [106]. Exposure to $PM_{2.5}$ can lead to respiratory and central nervous system disorders, blood disorders, and cancer [107]. Therefore, it is imperative to tackle $PM_{2.5}$ to improve air quality. However, conventional filters [108, 109], made from petroleum-based materials, pose a risk of secondary pollution due to their non-degradable properties. Cellulose (a natural polymer) offers superior adsorption capacity, chemical resistance, and flexibility, making it a promising alternative to petroleum-based polymers in the production of biodegradable air filters [110]. However, traditional cellulose-based filters have limitations such as poor gas adsorption capability and susceptibility to bacterial infections [111]. Therefore, reducing air pollution requires the development of an effective and sustainable air filter membrane that can capture and degrade $PM_{2.5}$.

Particle filtering membranes should have a high affinity, stability, robust porosity connectivity, and a sizable specific surface area [112]. Metal-organic frameworks (MOFs) coated electroret filters (E-MOFilters) are a new and promising technology that can effectively remove both particulate matter (PM) and volatile organic compounds (VOCs) [113]. E-MOFilters have demonstrated an 85% efficacy in PM filtering and a 90% efficiency in toluene adsorption [61]. It is worth noting that E-MOFilters are chiefly responsible for reducing VOCs levels through adsorption with the ability to solely absorb VOCs contaminants. Although the non-destructive adsorption technique used in E-MOFilters is simple, the adsorption quantity may decrease over time due to saturation and concentration gradient desorption [114]. Another possible solution to disrupt VOCs is the development of photocatalytic oxidation method proposed by Fukushima and Honda in 1972 [115]. Photocatalysts are a promising solution for decomposing VOCs into harmless products, such as water and carbon dioxide. Among the various photocatalysts, because of its great stability, robust resistance to corrosion, and non-toxicity, titanium dioxide (TiO_2) stands out among the other photocatalysts [116]. High excitation energy, low electron-to-oxygen transfer rate, and high electron pair recombination rate are some of the variables that restrict its photocatalytic efficacy. In order to get around these restrictions, scientists have been investigating the possibility of using metal-organic framework (MOF)/semiconductor composite materials, such as MIL-100(Fe)/TiO_2, ZIF-8/ZnO, ZIF-8/TiO_2, UiO-66-NH_2/TiO_2, UiO-66-NH_2/g-C_3N_4, MIL-125(Ti)/GO, MIL-125-NH_2/BiOCl, and MIL-125-NH_2/Bi_2WO_6, as possible photocatalysts to break down volatile organic compounds (VOCs) [117].

4.1 MOFs design principle for adsorption and conversion of VOCs and $PM_{2.5}$

Through the process of intercepting and filtering, MOF can absorb particles and other hazardous gaseous pollutants. This results in enhanced filtration effectiveness, which can be further improved depending on pore size [118]. Composite materials comprising semiconductor particles and MOFs have been developed to act as photocatalysts that photodegrade VOCs molecules. MOFs have an abundance of adsorption sites to retain a significant quantity of VOCs, while semiconductor particles act as catalysts to photodegrade them. By combining graphene oxide (GO) with NH_2-MIL-125 (Ti) using a microwave heating technique, a heterojunction photocatalyst was created. The produced 10-GO/NH_2-MIL-125 (Ti) showed significant improvement in photocatalytic efficiency for gaseous acetaldehyde. According to the results, the composite materials enhanced photocatalytic activity may be attributed to increases in visible light absorbance, carrier density, charge transfer efficiency, and a decrease in electron-hole recombination rate.

Huang and colleagues created TiO_2@NH_2-MIL-125 as a photocatalyst to remove formaldehyde (Table 3). Comparing the photocatalytic removal rate of HCHO to that of pure TiO_2 and NH_2-MIL-125, the findings showed a considerable improvement after treatment (Fig. 4c), with a 90% removal rate [70]. Zhang used solvent evaporation to create TiO_2-UiO-66-NH_2 nanocomposites in a different work (Fig. 4d) (Table 3). Because of the strong adsorption capacity of NH_2-MIL-125, the high dispersibility of TiO2, and the effective interfacial charge transfer synergy between TiO_2 and NH_2-MIL-125, the nanocomposite photocatalysts demonstrated a conversion efficiency of 72.7% for toluene, which is 9.7 times greater than UiO-66-NH_2 [71]. Moreover, acetaldehyde conversion efficiency was greater than UiO-66-NH_2. These findings show that heterojunction formation can greatly enhance the performance of MOF/semiconductor photocatalysts in VOCs removal.

A polyacrylonitrile@TiO_2/zeolite imidazolic acid framework-8 (PTZ) hybrid membrane was used by Yang et al. to study the performance of $PM_{2.5}$ filtration and photodegradation [67]. The results showed that the enhanced PTZ membrane greatly increased the capture efficiency of $PM_{2.5}$ and that the mixed structure produced by PTZ showed greater $PM_{2.5}$ degradation effectiveness compared to PT, with an increase from 66% to 85%. In the meantime, Ma studied Ag-MOFs@CNF, where ZIF-8 and Ag-MOF crystals were successfully deposited on the cellulose fiber

surface, as demonstrated by the ZIF-8 filter, SEM, and EDS data. The intermediate layer of ZIF-8 filter material was observed to have a denser and smaller pore structure than the higher and lower layers (Fig. 4b). This is because ZIF-8 crystals and Ag-MOFs can mix to form a complex, dense composite filter porosity structure (Table 3).

4.2 Adsorption and transformation mechanism

Yang et al. study [67] contrasted the QF of PTZ-1 with that of other air filters (Fig. 4a). PTZ-1 had exceptional $PM_{2.5}$ filtering ability, according to the study (Fig. 4e). Ma et al. [69] employed $PM_{2.5}$ and PM_{10} as benchmarks to evaluate filter effectiveness. It was shown that pure cellulose filters were less effective in removing $PM_{2.5}$ and

◂**Fig. 3** **A** Fe^{2+}-MOF-5: **a** Illustration of the secondary MOF-5 building unit in which Fe^{2+} replaces one of the Zn^{2+} ions to produce Fe^{2+}-MOF-5. Reprinted with permission from the source [55], Copyright 2015, American Chemical Society. **b** NO disproportionation at Fe^{2+} nodes. Reprinted with permission from the source [55], Copyright 2015, American Chemical Society. **c** The green, blue, and gold X-ray adsorption spectra of Fe-MOF-5 are shown. Reprinted with permission from the source [55], Copyright 2015, American Chemical Society; **B** $[[Zr_6O_4(OH)_4(AA)_6]_2(cal)_3$: **a** Structure of the novel MOF $[Zr_6O_4(OH)_4(AA)_6]_2(cal)_3$ in partial crystal form. Reprinted with permission from reference [56], Copyright 2018, Angewandte Chemie International Edition. **b** Structure representation and basic grid topology of 2-methylpropyl hydrogen carbonate and connectors. Reprinted with permission from reference [56], Copyright 2018, Angewandte Chemie International Edition. **c** N_2 adsorption isotherm of sample $[Zr_6O_4(OH)_4(AA)_6]_2(cal)_3$ extracted by asoxet at 77 K. Reprinted with permission from reference [56], Copyright 2018, Angewandte Chemie International Edition; **C** MFM-300(Al): **a**, **b** The interaction between MOF and guest molecules at binding sites I and II, and **c** Formation of a 1D spiral chain in the MFM-300 (Al) channel. Reprinted with permission from reference [57], Copyright 2018, Nature Materials. **d** The MFM-300 (Al) adsorption isotherm for NO_2 and other gases at 298 K. Reprinted with permission from reference [57], Copyright 2018, Nature Materials. **e** Equal volume adsorption heat (Qst) and entropy of NO_2 adsorbed by MFM-300 (Al) (ΔS). Grey is C, Blue is N, White is H, Red is O, and Green is Al. Reprinted with permission from reference [57], Copyright 2018, Nature Materials

PM_{10} than composite filters like MOFs@CNF and CF, particularly Ag-MOFs@CNF and the ZIF-8 filter (Table 3). This is attributed to bi-component MOFs, which improve the filter-PM interaction, thus increasing the filtering effectiveness of the composite filter [119]. The gradient filtering method in the multilayer structure can intercept more particles through the complex zigzag channels for particle passage, thereby increasing the frequency of effective collisions between the filter and particles [120]. ZIF-8 nanocrystals increase the filter's specific surface area and improve its filtration capabilities [83]. Therefore, the multilayer Ag-MOFs@CNF filter offers a great deal of promise for PM removal.

ZIF-8 nanocrystals are known for their rich adsorption sites and specific surface areas that are crucial for gas adsorption and capture. These crystals possess organic and open metal adsorption sites that enhance the ability of the composite filter to adsorb gases significantly. ZIF-8 crystals really have a specific surface area of 1545.2 m^2g^{-1}, which is 126 times more than that of a filter element made entirely of cellulose. Ag-MOFs@CNF has been significantly enhanced by the addition of ZIF-8 nanocrystals, making it a more effective gas adsorption material. Among the three adsorption sites, it is also notable that the nitrogen adsorption process begins at the metal centers (zinc). The gas fills all the holes in the ZIF-8 crystal as the pressure increases by diffusing onto the organic ligand. This enhances the overall performance of the composite filter, making it an excellent choice for gas adsorption and capture [83].

The mechanical characteristics of filter materials are primarily determined and crucially assessed by their compression performance, particularly Ag-MOFs@CNF and bicomponent MOFs. ZIF-8 filter exhibits better compressive strength. The inclusion of MOF crystals in composite filters leads to richer active sites and structural optimization, which enhance cellulose molecular chain interactions [121]. ZIF-8 crystals demonstrated excellent gas adsorption capacity for CO_2, CH_4, and N_2 in earlier studies by Russell et al. [122]. Moreover, MOF filters can selectively capture and adsorb SO_2/N_2 mixtures [123]. The findings suggest that the gas adsorption capability of Ag-MOFs@CNF and ZIF-8 air filters is highly effective. Based on the above, this filter has the potential to become a multifunctional air filter that can absorb toxic gases and purify air.

5 Other air pollutants separation using MOFs

5.1 Vehicle exhaust separation using MOFs

The extensive utilization of automobiles has resulted in elevated levels of exhaust emissions, which pose a severe threat to human health. The volatile organic compounds and nitrogen oxides present in the exhaust gas can quickly contaminate the atmosphere and contribute to air pollution. Moreover, they can cause respiratory problems among people [124]. In recent years, the vigorous development of new energy electric vehicles will reduce some carbon emissions, but the taxi in electric vehicles will even lead to the increase of NO_2 concentration and the rise of CO, SO_2, O_3, and particulate matter levels, resulting in a decline in air quality [125]. The handling of automobile emissions has gained significant attention in recent years as it affects public health [126]. Studies have demonstrated that exposure to benzene toxicity can result in symptoms like headaches and neurasthenia, as well as genetic damage. Long-term exposure to benzene can lead to human anemia [127], while many benzene can cause photochemical smog and secondary pollution in cities [128].

During vehicle operation, the combustible mixture undergoes a series of chemical reactions influenced by various factors, such as high temperature, high pressure, and electric sparks. These reactions produce nitrogen oxides (NO_x) [129], which comprise a family of toxic gases with varying toxicity levels [130]. NO_x present in the atmosphere can also contribute to acid rain [131]. Petroleum commonly contains elemental sulfur, which when burned, produces sulfur dioxide that dissolves in water to form sulfite. This can accelerate acid rain formation, which can harm animals and plants [132] as well as corrode and damage buildings [133]. Additionally, in the presence of sunshine, nitrogen

Table 3 Performance summary of MOFs in $PM_{2.5}$ capture and VOCs degradation

MOF	Application	Key properties	$PM_{2.5}$ capture	VOCs degradation	Reference
10-GO/NH2-MIL-125(Ti)	Photocatalyst	Increased visible light absorbance, high carrier density	N/A	Acetaldehyde	[70]
TiO2@NH2-MIL-125	Photocatalyst	Strong adsorption, high dispersibility	N/A	Formaldehyde (90% removal)	[70]
TiO2-UiO-66-NH2	Photocatalyst	Strong adsorption, effective charge transfer	N/A	Toluene (72.7% conversion)	[71]
PTZ (PT@TiO2/ZIF-8)	Membrane filter	Multilayer structure, dense pore size	High efficiency	PM2.5 (66% to 85% degradation)	[67]
Ag-MOFs@CNF (ZIF-8, Ag-MOFs)	Membrane filter	Multilayer structure, rich adsorption sites	High efficiency	N/A	[69]
ZIF-8	Filter material	High-specific surface area, abundant adsorption sites	N/A	N/A	[83]

oxides in exhaust gas can combine with hydrocarbons to create photochemical smog [134], which in turn generates secondary pollutants. This can lead to the development of respiratory system diseases and eye irritation [135], as nitrogen oxides and sulfur oxides can enter the body through the respiratory tract during human respiration, causing lung and respiratory ailments. Furthermore, exposure to nitrogen oxides can cause developmental delays in children [136]. Since their inception in 1974, ternary catalysts have undergone continuous improvement [137–139] and have become an essential component of automobile exhaust control [140]. Table 4 shows the effect of some catalysts in the treatment of automobile exhaust gas.

5.1.1 MOFs design principles for vehicle exhaust separation

Photocatalysis is an emerging technology that offers several economic benefits. Among the many photocatalysts, titanium dioxide (TiO_2) is a popular choice for water splitting to produce hydrogen under ultraviolet light. Although TiO_2 demonstrates excellent photocatalytic performance and has been widely researched [115], its wide bandgap restricts its photo response to only ultraviolet light. To overcome this limitation, researchers have explored semiconductor photocatalysts with appropriate bandgaps in recent years [145]. Because of its special qualities—such as their porous structure, large-specific surface area, high thermal stability, and exceptional catalytic activity—porous coordination polymers, or MOFs, have become intriguing materials for a range of applications [146]. However, certain practical issues such as low sunlight utilization and limited photocatalytic activity [147], have hindered the full-scale utilization of MOFs. As a result, researchers have explored various methods to enhance the photocatalytic activity of MOFs through modifications. Many studies have been conducted to investigate the effectiveness of modified MOFs in addressing these issues. In a recent study, to facilitate photocatalytic oxidation, Liu et al. [148] used the UiO-66-NH_2@MIL-101 (Fe) heterostructure as a catalyst. Under visible light irradiation, Zhang et al. [149] used solvothermal synthesis to create NH_2-MIL-101 (Fe) hexagonal microspheres, which they then used to remove gaseous toluene. It was found that the addition of NH_2 to MIL-101 (Fe) enhanced the visible light absorption. MOF photocatalysts provide a variety of benefits over other catalysts, including improved structural stability from the organic and inorganic components of the framework, increased light adsorption range from its high porosity, and effective encouragement of rates for light-generated e^- and h^+ separation and transfer due to its adjustability.

5.1.2 Adsorption and transformation mechanism of vehicle exhaust separation

Mahy et al. [150] conducted a study on a photocatalytic coating that degrades NO_x and organic compounds in exhaust gas. They tested the performance of the sample for photocatalytic degradation of NO_x and found that most samples had degradation rates between 10% and 45%. Ma et al. [151] mixed TiO_2 nanoparticles into asphalt and heated the mixture to 170 °C in order to get samples that had degrading activity for NO_x and CH. Nano TiO_2 coating materials have been produced by Yu et al. [152] to enhance the activity and stability of TiO_2 on road surfaces for relevant applications. Anatase-type nano-TiO_2, activated carbon powder, silane coupling agent, and deionized water were used to make the materials. Sodium dodecylbenzene sulfonate was added as a surfactant at different mass ratios to the road coverings. The study discovered that a mass ratio of around 1:2 between nano-TiO_2 and surfactant maximized catalytic degradation impact. Similarly, Singh et al. [153] optimized the parameters for loading TiO_2 on asphalt pavement to degrade SO_2 and NO_2, resulting in significant practical effectiveness. Wang et al. [154] employed an innovative

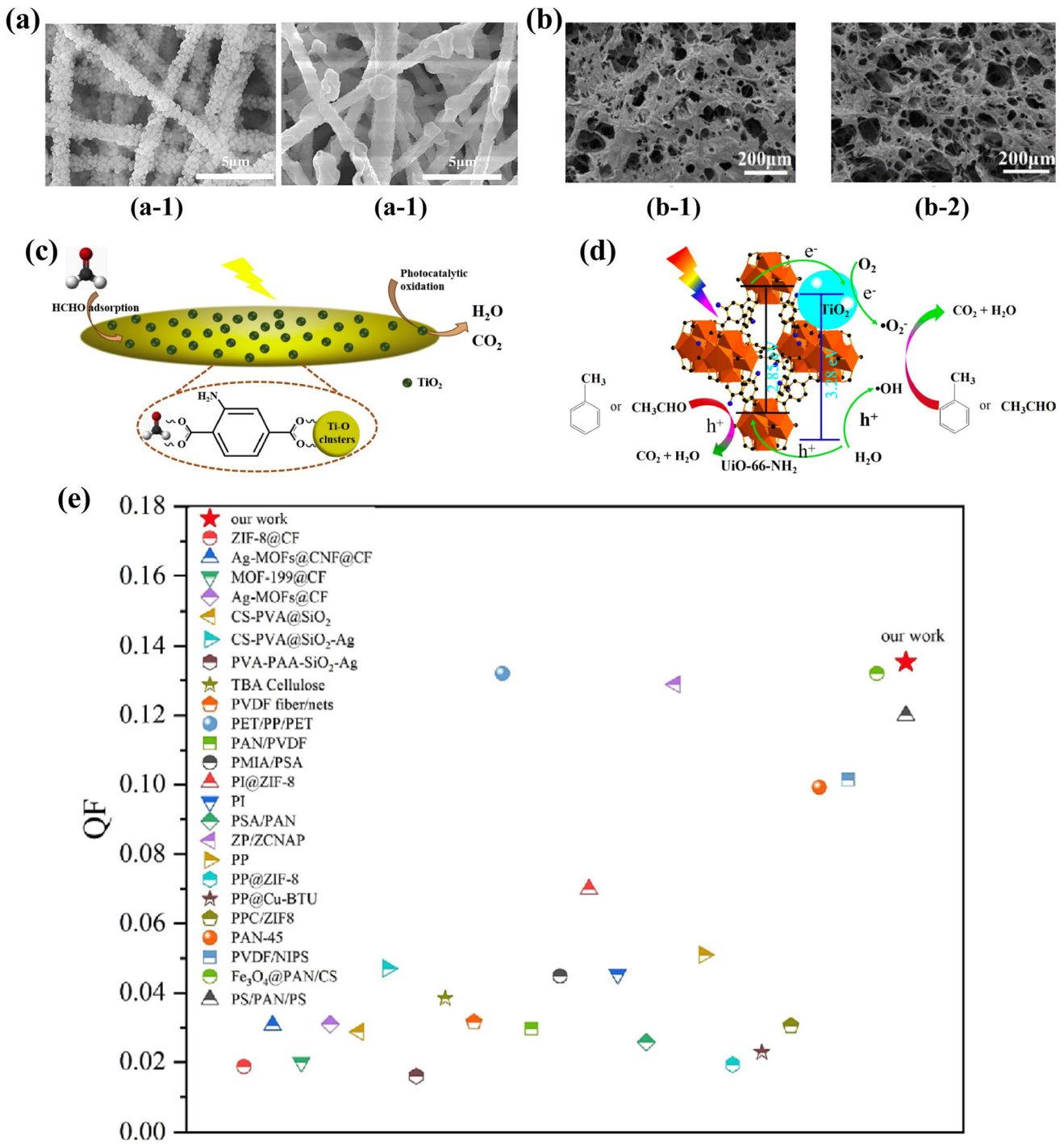

Fig. 4 **a** $PM_{2.5}$ SEM pictures before and after PTZ filtering (a-1, a-2). Reprinted with permission from [67], Copyright 2023, Journal of Colloid and Interface Science.; **b** (b-1) Ag-MOFs@CNF @SEM images of CF crystals, (b-2) ZIF-8@CNF and SEM images of CF crystals. Reprinted with permission from [69], Copyright 2019, Carbohydrate Polymers; **c** Schematic diagram of TiO_2@NH_2-MIL-125 composite. Reprinted with permission from [70], Copyright 2019, Applied Catalysis B: Environmental; **d** Composite schematic diagram of TiO_2-UiO-66-NH_2 Reprinted with permission from [71], Copyright2020, Chemical Engineering Journal; **e** QF for air filters such as PTZ-1. Reprinted with permission from [67], Copyright 2023, Journal of Colloid and Interface Science

approach of laying finely ground TiO_2 cement mortar on the road surface, then drying it and applying epoxy resin to fix the catalyst on the road surface to improve the wear

Table 4 Part of the catalyst used to treat automobile exhaust

Pollutant category	Pollution concentration	Catalyst	Efficiency (%)	Ref.
CO	ND	Pt-TiO_2P25	8.2	[141]
CO_2	ND	SIFSIX-Ni-dpt	19.65 mmol g^{-1}	[142]
Hydrocarbon(C_3H_6)	560 ppm	Pt-TiO_2P25	77.3	[141]
Formaldehyde, acetaldehyde and trichloroethylene	1000 ppm	DAPs	5.10 µmol s^{-1}. g_{cat}^{-1}	[143]
Isopropanol	1.8-14.6 ppm	TiO_2	99	[144]
SO_2	ND	MFM-601	12.3 mmol g^{-1}	[47]

resistance of the photocatalyst on the road surface. The NO_x removal rate, road wear resistance, and slip resistance were assessed, and the results showed that effective NO_x degradation could be achieved.

5.2 Coal-fired flue gas separation using MOFs

Coal combustion leads to the release of CO_2 and SO_2 as primary air pollutants. Global temperature increase is attributed to CO_2 emissions, with an addition of 0.2 °C every decade. The emissions of coal-fired exhaust gas, represented by the energy intensive steel industry, account for 7% of the global anthropogenic carbon dioxide emissions due to the combustion of a large amount of coal in the production process [155]. SO_2 emissions are also a severe concern, which can cause acid rain and environmental damage, leading to lung diseases in humans. Carbon capture and storage technology is used to lessen the effects of CO_2 emissions, which involves the extraction of CO_2 from the production point source and its injection underground for long-term storage. Conventional carbon capture technology involves the selective absorption of CO_2 by aqueous amine solutions, which form ammonium carbamate and ammonium bicarbonate. However, this process has several limitations such as amine volatilization, thermal degradation, and oxidative degradation, with low adsorption capacity and high cost. Therefore, the development of porous materials with high selectivity and adsorption capacity for gases is crucial for reducing atmospheric pollution. MOFs are a promising solution that can cater to these specific requirements [51], as shown in Fig. 5a.

5.2.1 MOFs design principles for coal-fired flue gas separation

In addition, Cui et al. [155] proposed a passive dual heat management strategy based on high latent heat and improved thermal conductivity. The mil-101 (Cr) ministry structure prepared has stable structure, high water absorption and desorption, and can spontaneously store and evaporate, taking away excess heat. In order to prove the high cyclic water absorption performance of mil-101 (Cr) under different conditions, they also explored the nitrogen adsorption isotherm of mil-101 (Cr), and compared with traditional adsorbents, the mil-101 (Cr) ministry obtained has better adsorption-desorption kinetics. MOF is a material produced from the self-assembly of organic ligand units and transition metals through coordination bonds. Compared to molecular sieves, MOF materials have a substantially wider specific surface area while maintaining the same morphology, structure, and controlled grain size [51, 158]. The main techniques for MOF regeneration include temperature swing adsorption (TSA), pressure swing adsorption (PSA), vacuum pressure swing adsorption (VSA), and their mixtures [159]. But to transmit pressure changes that cause adsorbed gas to escape from the wall, VSA and PSA need a lot of electrical energy [160]. Despite variable temperatures operations can utilize the waste heat generated by coal-fired sources, however, the use of microporous MOF adsorbents on a large scale is impractical due to their superior insulation properties. The poor heat conductivity of MOFs increases the cycle time significantly. Moreover, they may interact with electromagnetic radiation present in the environment, leading to structural changes at both small and large scales. Preloading guest molecules may also result in their expulsion from the pore, as shown in Fig. 5b. Britt et al. [79] developed a one-pot approach to manufacture MOF with different organic ligands. However, some of these frameworks exhibit low hydrothermal stability and compete with water during the adsorption process, leading to the collapse of the adsorbent structure and a decrease in saturation adsorption capacity.

5.2.2 Adsorption and transformation mechanism for coal-fired flue gas separation

Gas adsorption and separation using porous materials is a widely utilized method that involves the mechanisms of molecular screening, thermodynamic equilibrium, molecular dynamics, and quantum sieving [161, 162]. Molecular screening selectively adsorbs different gases based on their shape and kinetic diameter, allowing molecules with a kinetic diameter equal to or less than the pore diameter

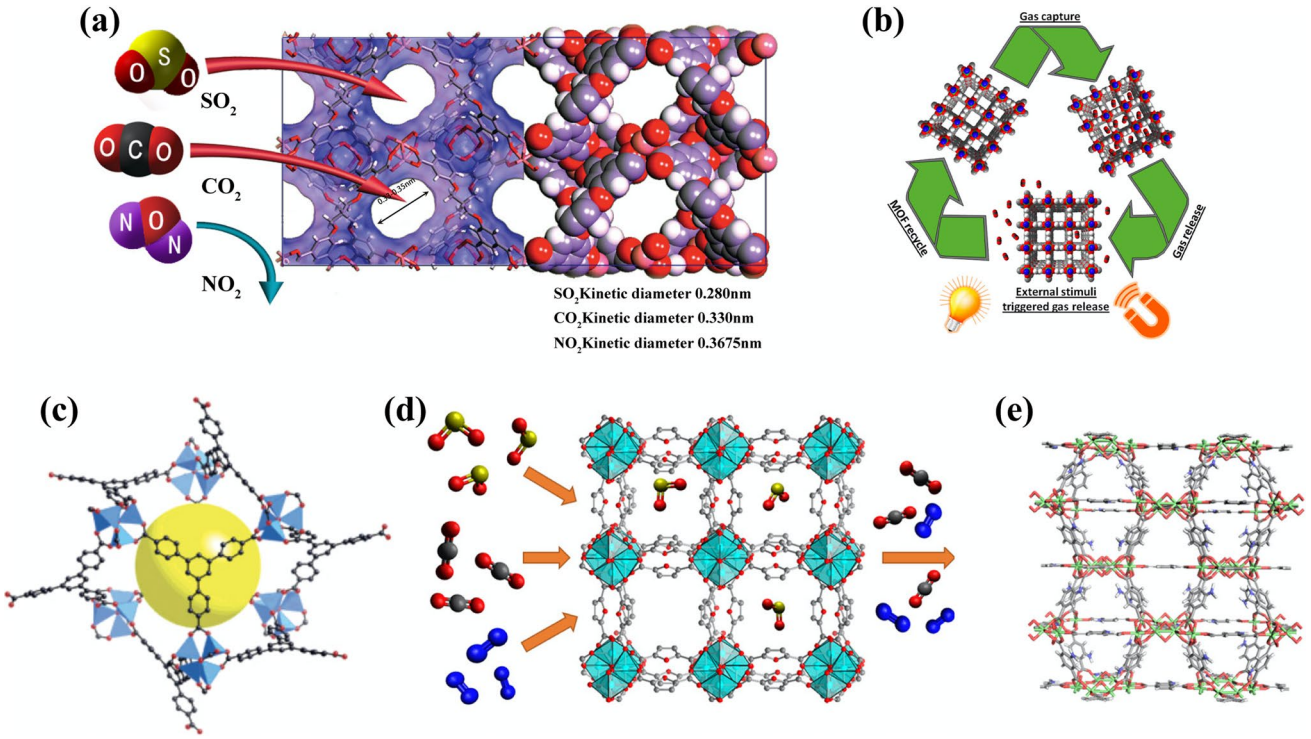

Fig. 5 **a** Schematic diagram of selective gas adsorption of MOF based on molecular sieve effect. Adapted with permission [156], Copyright 2020, Science of The Total Environment.; **b** Schematic diagram of recoverable stimulus response MOFs regulated by external stimuli for gas adsorption and release. Reprinted with permission from [157], Copyright 2017, American Chemical Society; **c** Molecular structure diagram of MOF-177. Reprinted with permission from [49]. Copyright 2005, Angewandte Chemie International Edition.; **d** The crystal structure of MIL-160. Reprinted with permission from [51], Copyright 2019, American Chemical Society.; **e** The crystal structure of NH_2-MIL-125 (Ti) [50]. Copyright 2017, American Chemical Society

to pass through. The effectiveness of molecular screening can be influenced by temperature, as certain adsorbents have pore sizes that are sensitive to temperature. For optimal results, it is recommended to utilize equilibrium separation when the gas mixture components can easily pass through the interior of the adsorbent and its pore size is appropriately large. The interactions between molecules and the adsorbent surface have a major impact on the quality of selective adsorption. Additionally, the characteristics of the adsorbent molecules impact their contact strength. For instance, magnetic susceptibility, quadrupole moment, permanent dipole moment, and polarizability [163]. Dynamic separation is employed when equilibrium separation is not feasible. Precise tuning of the adsorbent pore size is crucial in dynamic separation, particularly when separating two molecules with varying dynamic diameters. In isotope separation, quantum sieving can be used to differentiate between guest molecules diffusion rates based on the compatibility of their pore widths with de Broglie waves.

5.3 Fuel exhaust separation using MOFs

Around 44% of global CO_2 emissions are a result of fuel combustion from sources such as coal, natural gas, and oil [164]. Over the past 100 years, the global average temperature has increased by 0.5 °C, and according to most global climate models, it will continue to rise by 1.5–3.0 °C over the next 100 years [165, 166]. So, it an urgent priority to capture CO_2 after combustion (Fig. 6a). For the past few decades, extensive studies have been conducted on CO_2 capture. Numerous carbon capture systems involving different techniques such as solid adsorption, electrochemical separation, low-temperature separation, and chemical adsorption of various solvents and membrane separation [171], nanofluids [172], ionic liquids [173], amino acid salt solutions [174], low-temperature separation, electrochemical separation, and solid adsorption have been widely researched. Danaci studied the effect of adsorption temperature on purity and recovery, as shown in Fig. 6e–f. This technology low energy usage and remarkable efficiency have drawn a lot of interest

[175]. MOF has recently shown promising potential for CO_2 removal and can provide superior CO_2 adsorption capacity under low CO_2 partial pressure [176].

5.3.1 MOFs design principles for fuel exhaust separation

Because of their vast surface area, varied architectures, and high porosity, MOFs are very excellent CO_2 adsorbents. These three-dimensional microporous crystal structures are composed of a network of metal ligands and coordination bonds that connect the ligands to the central metal atom [177]. Due to the existence of these coordination bonds, MOFs are also known as coordination networks or coordination polymers at times [178, 179]. In MOF synthesis, the angstrom-level pore size and channel enable CO_2 storage [180]. Under high pressure, MOFs can store up to 12 times more CO_2 than empty containers, making them a significant asset to carbon capture and storage. Following the efficient capture of CO_2 by MOF, it is noteworthy that additional molecules will absorb and store it in the available pores and channels [177, 181]. This method is practical when dealing with confined spaces [182]. To optimize capture efficiency, MOFs with high CO_2 adsorption at low pressure are recommended. Darute et al. [76] have validated the carbon dioxide capture efficiency of polyethylene imine (PEI) injection into MIL-101. The adsorption capacity of carbon dioxide at 400 ppm is 1.0 mmol g^{-1}. Applications of MOF are numerous and include, but are not limited to, gas storage, CO_2 catalysis, CO_2 capture, VOCs detection, and gas purification and separation [183–185]. Currently, the physical adsorbents represented by MOF can adsorb gases of different concentrations. Figure 6d illustrates the adsorption capacity of several MOFs.

5.3.2 Adsorption and transformation mechanism for fuel exhaust separation

Research on the extraction of CO_2 gas from a CO_2 and N_2 mixture in Mg-MOF-74 was carried out by Mansour and Qasem. In their work, the TSA process was numerically simulated utilizing a four-step cycle involving feeding, rinsing, heating, and cooling [77]. Similarly, PSA operates by adsorbing the target gas from the gas mixture stream, followed by a vacuum pump that blows down the gas CO_2 flow. The light product is next pressured using the adsorption step's output flow after the gas is released countercurrently at the free end. The process involves high-pressure operation during the adsorption step. In CO_2 mixture adsorption by the MOF, the mixture enters from the bottom and is adsorbed at the top. The exhaust process operates at medium pressure, utilizing a vacuum pump to exhaust N2 from the top, resulting in a higher CO_2 concentration. These four methods were also used by Rajagopalan and Rajendran [190] to gather CO_2 and create 94.8% pure CO_2 from CO_2 and N_2 combined with zeolite 13X as an adsorbent [191]. Adhikari and Lin [169] looked at how activated carbon (AC) affected MOF-74-Ni and MOF-74-Co ability to adsorb CO_2. The CO_2 adsorption rates of both modified MOFs were greater than those of the original structure. This is attributed to partially negatively charged oxygen atoms interacting with partially positively charged Pd atoms in polar CO_2. Figure 6c depicts the CO_2 of the original and upgraded structures at low pressure. Hu et al. [168] looked into absorption properties of pn-Mg2(dobpdc), mpn-Mg2(dobpdc), and dmpn-Mg2(dobpdc) showing CO_2 absorption between 2.7 and 4.1 mmol/g at 150 mbar and at 40 °C. Among these pn-Mg2(dobpdc) containing 2 amine groups showing highest absorption rate around 4.1 mmol/g and dmpn-Mg2(dobpdc) that has 2 methyl group and no free amine shows lowest absorption rate. Secondary amines have ability to interact with CO_2 through hydrogen bonding and enhance CO_2 absorption. This interaction was particularly evident in the high absorption rate demonstrated by pn-Mg2(dobpdc) compared to mpn-Mg2(dobpdc) that has one amine and one methyl, and dmpn-Mg2(dobpdc) no amine and two metyl groups (Fig. 6b).

The mechanism for capturing CO_2 depends on the interaction between CO_2 and the adsorbent [187, 192]. Usually, dynamic sieving is used when the gas size is comparable to or less than the CO_2 molecules molecular size [159, 187]. MOF is a selective adsorbent for CO_2 in the flue gas stream, allowing CO_2 capture and separation. Danaci et al. [170] suggest higher CO_2 capture capacity and ease of regeneration of Mg-MOF-74 over UTSA-16 (Fig. 6e and Fig. 6f). The two adsorption sites of the MOF enhance its affinity for CO_2, resulting in better adsorption efficiency. Belmukhout et al. [187] have studied various MOF types including Mg-MOF-74, SIF6-3-Zn, and SIF-6-3-Cu, with CO_2 adsorption rates of 0.08 mmol/g, 0.13 mmol/g, and 1.24 mmol/g, respectively. The incorporation of hydroxyl groups on the Mg site of Mg-MOF-74 (Fig. 6e) significantly enhances CO_2 adsorption in the channel. MOFs with narrow pore sizes, which are selectively used for gas separation based on gas dynamic diameter, exhibit rapid adsorption kinetics. The separation of gases is primarily driven by gas dynamics. Compared to gases like CH_4, H_2, and N_2, CO_2 molecules with hole sizes less than 40 nm have a larger potential for separation [187]. Devic and Serre [186] conducted a study on various MOF structures based on M^{3+} cations. They identified one-dimensional pores of MIL-53 which resulted in the rhombic shape of MIL-53, while MIL-68 exhibited a triangular and hexagonal shape as depicted in Fig. 7a–d.

It has been discovered that MOFs are very efficient catalysts for the catalytic conversion processes of CO_2. MOFs can be utilized as a catalyst to reduce CO_2 to methanol, according to recent studies [78]. Development of functionalized MOFs like UiO-68-NHC has been created by

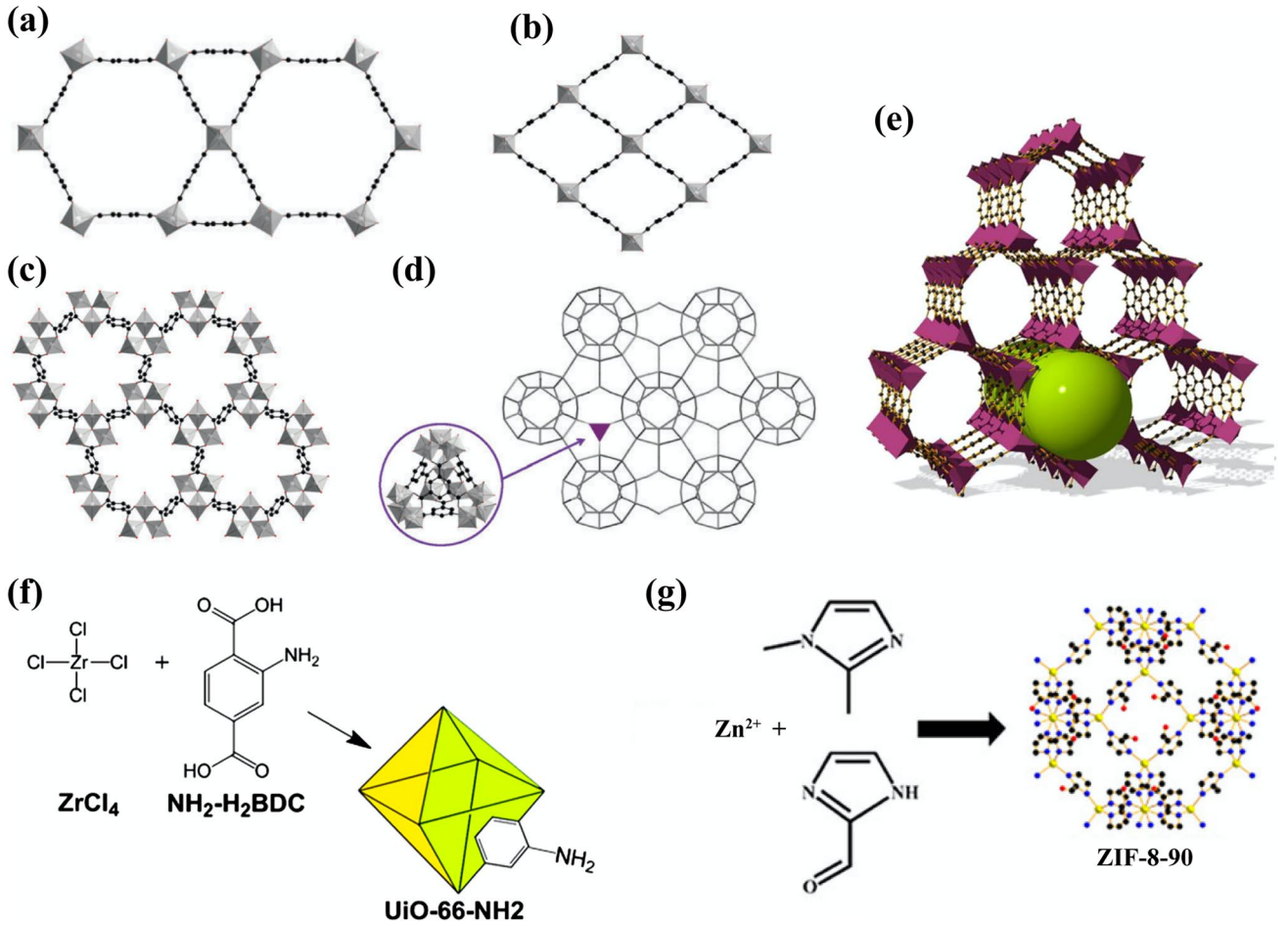

Fig. 7 **a**–**d** Structural framework of M^{3+} dicarboxylate and tricarboxylate systems in MIL-53, MIL-68, MIL-88, and MIL-100. Reprinted with permission from [186], Copyright 2014, Chemical Society Reviews. **e** Mg-MOF-74 structural framework. Reprinted with permission from [187]. Copyright 2016, Chemical Engineering Journal. **f** Molecular structure and framework diagram of UiO-66-NH_2. Reprinted with permission from [188]. Copyright 2016, Journal of Colloid and Interface Science. **g** Molecular structure diagram of ZIF-8-90. Reprinted with permission from [189]. Copyright 2021, American Chemical Society

combining imidazole bromide ligands with MOFs that include metal-free n-heterocyclic carbon (NHC). High yields of methanol have been produced using UiO-68-NHC capacity to transport hydrogen from silane to CO_2. After eight cycles, the yield of the MOF immobilized NHC catalyst is 90%, and it has a good selectivity for the necessary product methoxysilane. Yang et al. [193] have also developed MOF based on Ni30 clusters, which has been found to significantly impact the catalytic conversion of CO_2 and epoxides to cyclic carbonates. Kurisingal et al. work [194] focused on the synthesis of Cu BTC/Zr UiO-66 binary MOFs for CO_2 cycloaddition with epoxides in a solvent-free setting. There is a noticeable conversion impact, according to the data. The binding of Zr and Cu in MOF shows 99% selectivity for ECH carbonates, while the binding of Br in tetrabutylammonium bromide exhibits 99% selectivity for ECH carbonates. This study binary MOFs has outstanding recyclability; even after six cycles, there is no loss of catalytic activity. Additionally, Xiang et al. studied the double ligand ZIF-8-90 (Fig. 7g) [195], it produced an effective CO_2 and ECH cycloaddition. Compared to ZIF-8, the double ligand ZIF showed better stability and selectivity, and even after three cycles, there was no appreciable decrease in catalytic activity.

5.4 Waste incineration exhaust gas separation using MOFs

With the rapid growth of the global economy and the increase in urbanization, there has been a significant surge in urban household waste [196]. As per recent statistics, urban household waste generation across the world is estimated to be around 1.6 to 2 billion tons [196, 197]. Common methods for treating such waste include sanitary landfills, composting, and incineration. However, incineration of urban household waste emits SO_x and NO_x, with NO_x being mainly composed of NO and NO_2. The emission of NO_x has significant

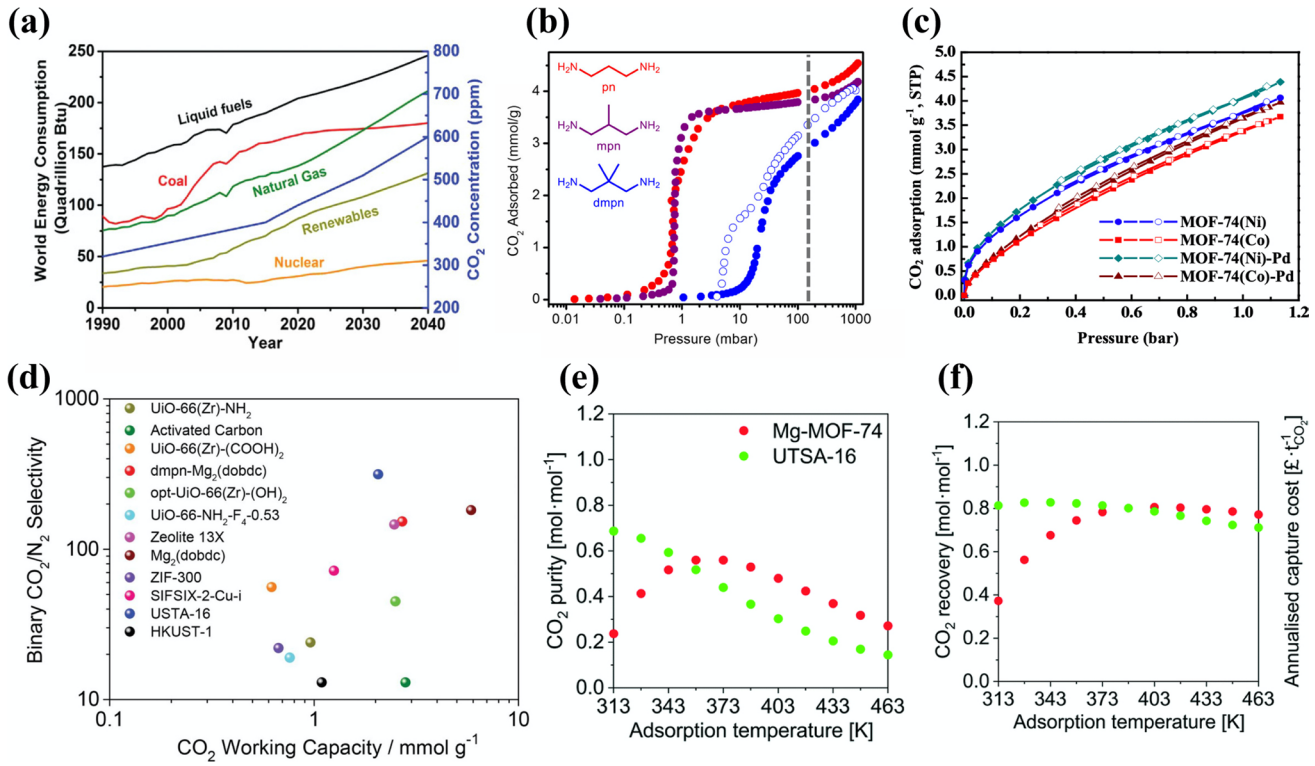

Fig. 6 **a** Changes in atmospheric carbon dioxide concentration caused by global energy consumption. Reprinted with permission from [167], Copyright 2018, Advanced Sustainable Systems.; **b** In pn⁻, mpn⁻, and dmpn–Mg2(dobpdc), the isotherms for CO_2 adsorption at 40 °C are displayed (desorption data presented with open circles). The estimated partial pressure of CO_2 (150 mbar) in coal flue gas is shown by the dotted line. Reprinted with permission from [168], Copyright 2017, American Chemical Society.; **c** At 298 K, the modified MOF-74 (Co) structure and the original MOF-74 (Ni) structure CO_2 adsorption isotherms (open loop denotes desorption). Reprinted with permission from [169], Copyright 2016, Chemical Engineering Journal.; **d** The capacity of different MOFs to absorb CO_2 after burning. Reprinted with permission from [167], Copyright 2018, Advanced Sustainable Systems.; The impact of various parameters on the cost and separation efficiency of UTSA-16 (green) and Mg-MOF-74 (red). Adsorption temperature impact on CO_2 purity **e** and recovery rate **f**. Reprinted with permission from [170], Copyright 2020, Molecular Systems Design & Engineering

implications for both human health and the environment [198]. Researchers have focused a lot of attention on porous MOFs materials because of their varied pore architectures, open metal sites, pore function, and changeable porosity. In recent times, these substances have demonstrated outstanding abilities in the adsorption and segregation of diverse liquids and gases.

5.4.1 MOFs design principle for waste incineration exhaust gas separation

Numerous adsorption pathways have been proposed with regard to chemical adsorption between MOF and SO_2/NO_x active sites [199, 200]. The adsorption process is significantly influenced by acid-base interaction, complexation, and hydrogen bonding [201]. Metal ions, or metal ion clusters, and ligands make up MOFs. Typically, organic units have two, three, or four terminal ligands [202]. Figure 8 illustrates some typical MOFs with solvents that serve as the primary template molecules for MOF [204]. Most metal cations can be involved in the formation of MOFs. During the formation process, the length of ligands of the same metal type only needs to be adjusted, and the framework pore size relies on the ligand length [205].

The use of the same ligand and different metal components allows for the preparation of multiple MOFs with similar properties [206]. MOFs have several uses, such as the adsorption and storage of CO_2 and the storage of hydrogen [207], steam adsorption [208], chemical separation [209], biomedical [210], and catalysis [211]. The pore surfaces of MOFs are easily modified and selectively adsorb guest molecules with specific functional groups. As an adsorption material, MOFs hold great promise and have been extensively studied for their ability to adsorb and remove various harmful substances from the environment [212]. Furthermore, interactions between the adsorbent and MOFs can be enhanced through central metal coordination with unsaturated sites [213], functionalized ligands [214], and loaded active substances [215], resulting in effective adsorption and removal of harmful compounds. Enhancing adsorption

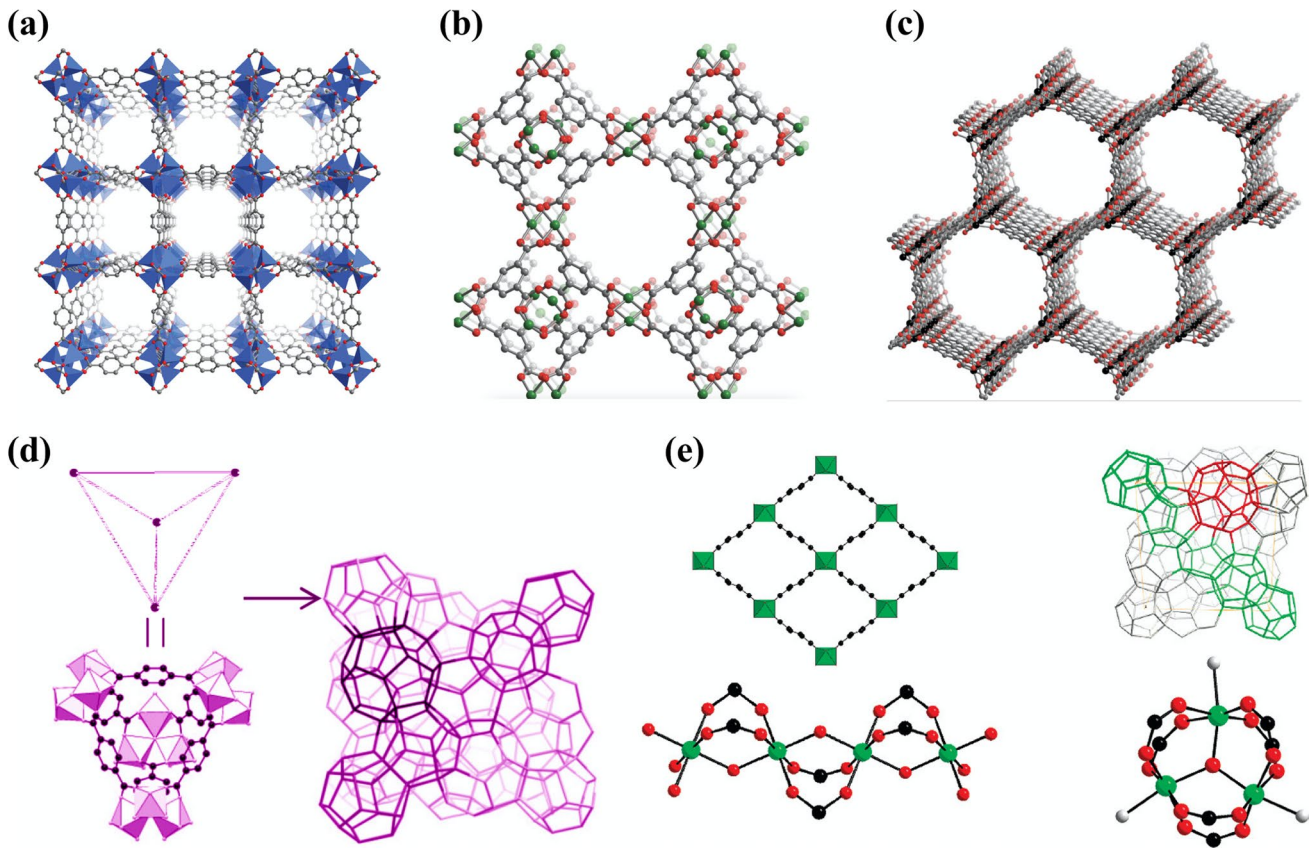

Fig. 8 **a** The composition of the metal organic framework MOF-5. Reprinted with permission from [159], Copyright 2012, American Chemical Society.; **b** The structure of the metal organic skeleton Cu BTC. Reprinted with permission from [159], Copyright 2012, American Chemical Society.; **c** The CPO-27 metal organic framework construction. Reprinted with permission from [159], Copyright 2012, American Chemical Society.; **d** Schematic diagram of the crystal structure of MIL-101. Each intersection point (right) of the illustrated structure corresponds to the superhedron of the chromium octahedral trimer and terephthalate moiety (left). Adapted with permission from [203], Copyright 2007, Advanced Materials. **e** Solid structures of MIL-47 (V) and MIL-53 (Al, Cr, Fe) (upper left). The structural schematics for MIL-101 (Cr) and MIL-100 (Cr) are shown in the upper right corner. The structures corresponding to the different inorganic components are shown in the diagram. At the end, water molecules and fluorine are shown in gray close together, while the metal, oxygen, and carbon atoms are shown in green, red, and black, respectively. Reprinted with permission from [80]. Copyright 2009, American Chemical Society

in various host-guest interactions is facilitated by acid-base, hydrogen bonding, complexation, and coordination [215–217] with open metal sites.

5.4.2 Adsorption and transformation mechanism for waste incineration exhaust gas separation

Removing dangerous gasses is essential to preserving clean air quality. MOFs have favorable functional groups, open metal sites, and pore sizes and porosities. These features greatly facilitate particular interactions with host adsorbents. Using pressure swing adsorption methods, Hamon and collaborators [80] carried out comparative tests on stable and readily regenerated MOFs. Polar H_2S molecules and inorganic chains of MIL-53s (Al, Cr) demonstrate strong interaction, causing the pores to seal at low pressure. As pressure increases, the pores reopen and disrupt the strong interaction between H_2S and OH (at the MOF metal position). As a result, weak host-guest interactions cause all pores to fill. The results from the adsorption isotherm study of MOF on H_2S are presented in Fig. 9a. The study carried out at high pressure (1.6 MPa) revealed that MIL-53 (Al) and MIL-53 (Cr) had maximal H_2S adsorption capabilities of 13.12 and 11.77 mmol g^{-1}, respectively. MIL-47 and MIL-53s have identical adsorption capacities for Al and Cr at high pressure with pores reopening, according to a different study on MIL-47, which is similar to MIL-53s but does not include OH groups. The study also revealed a Type-I isotherm for H_2S adsorption.

Petit and Bandosz [218] conducted a study on the adsorption of NO_2 NH_3, and H_2S from the environment using composite materials made of MOF and graphite compounds. According to the study, new holes may form at the interface between the carbon layer and the MOFs as a result of the

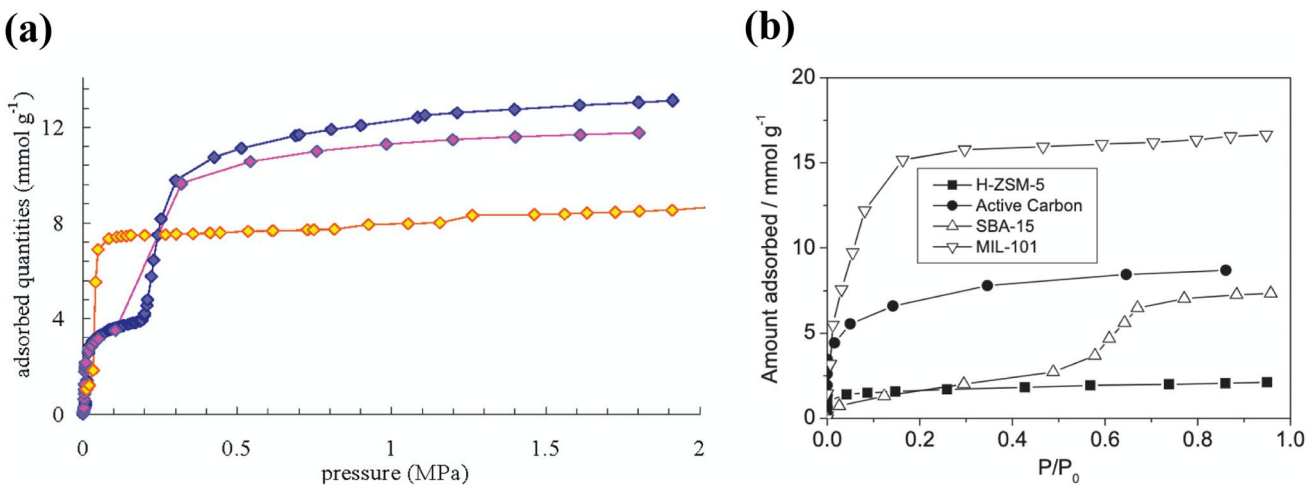

Fig. 9 **a** MIL-53 (Fe), MIL-53 (Cr), and MIL-53 (Al) adsorbed amounts of hydrogen sulfide at 303.1 K at pressures up to 2 MPa. Yellow: MIL-53 (Fe), Pink: MIL-53 (Cr), and Blue: MIL-53 (Al). Reprinted with permission from [80]. Copyright 2009, American Chemical Society.; **b** MIL-101, SBA-15, activated carbon, and HZSM-5 benzene adsorption isotherms. Reprinted with permission from [203], Copyright 2006, Advanced Materials

interaction between open metal sites and oxygen groups, producing composite materials with different properties. The experiment revealed that the GO/Cu-BTC composite material demonstrated a 12% improvement in NH_3 adsorption, 50% improvement in H_2S adsorption, and 4% improvement in NO_2 adsorption when compared to pure Cu-BTC.

Dathe et al. [219] have demonstrated that the adsorption of SO_2 by Cu-BTC impregnated with $Ba(CH_3COO)_2$ leads to the formation of small barium salt microcrystals inside Cu-BTC pores, thereby causing partial damage to the structure. The adsorption of SO_2 at high temperatures exceeds the stoichiometric capacity due to chemical bonding between metal cations and SO_2, leading to the formation of copper sulfate. As a result, Cu-BTC exhibits superior adsorption capacity at low temperatures. It has been demonstrated by Yazaydın et al. [220] that the inclusion of open metal sites in the Cu-BTC framework containing 4 wt% water molecules may considerably increase the capture ability of CO_2 and selectivity to N_2 and CH_4. Using a series of identically structured MOF of M-CPO-27s, Dietzel et al. [221] investigated the impact of metal centers on adsorption capacity and CO_2 adsorption selectivity. The results of the investigation show that at 298 K and high pressure (50 bar), the CO_2 adsorption rate of CPO-27 (Ni) is 51 wt%, and at 298 K and high pressure (50 bar), the CO_2 adsorption rate of CPO-27 (Mg) is 63 wt%.

According to Caskey et al. [222], at 1 atm, the CO_2 adsorption rates of CPO-27 (Co) and CPO-27 (Mg) were 30.6% and 35.2%, respectively. The use of small and uniform particles obtained by ultrasonic or microwave heating improves CO_2 adsorption [223, 224]. A total of 350 mg g^{-1} of CO_2 was adsorbed by ultrasonically produced CPO-27 (Mg) at 298 K, demonstrating a high adsorption isotherm [225]. MOFs functionalized with amine enhance CO_2 adsorption through acid-base or electrostatic interactions. Jhung et al. [203] evaluated the adsorption of benzene by MIL-101 (Cr), which has a gas phase adsorption capability of 16.7 mmol g^{-1}. Their findings reveal that MIL-101 (Cr) has an adsorption capacity 5.5 times higher than SBA-15, 8.7 times higher than H-ZSM-5, and 2 times higher than activated carbon (Fig. 9b), owing to its large porosity. The microwave irradiation method is used to produce MIL-101 (Cr) in liquid-phase adsorption [226]. In addition, An et al. [227] based on high latent heat properties along with improved thermal conductivity have proposed a passive dual thermal management strategy. The prepared MIL-101 (Cr) MOF exhibits structural stability along with high water absorption/desorption capacities enabling spontaneous storage/release cycles which effectively dissipate excess heat. To demonstrate its superior cyclic water absorption performance under varying conditions; they also investigated nitrogen adsorption isotherms which revealed superior kinetics compared to traditional absorbents.

6 Conclusion

Undeniably, significant advancements have been made in global technology. Despite substantial progress in controlling air pollution, it remains a complex and multifaceted challenge, posing serious threats to public health and potentially impacting life expectancy. Of particular concern is the widespread issue of haze formation, which has multiple complex causes and diverse components. To address this

issue effectively, comprehensive solutions have been developed for different gaseous pollutants. These encompass a range of treatment technologies aimed at adsorption, purification, and separation of various pollutants to enhance air quality and improve the human living environment while reducing incidence rates and extending lifespan.

SO_2 has extremely complex chemical properties and is often present in the atmosphere. Therefore, we have summarized a series of treatment plans here. Metal-organic frameworks (MOFs) including ZIF-8, HKUST-1, MIL-101, and UiO-66 have been the subject of extensive study, and the results indicate that these MOFs may effectively adsorb and convert SO_2. As crucial, other hazardous gases like nitrogen dioxide (NO_2) may also be addressed using MOFs because of their large surface area and versatile features. However, it is crucial to overcome challenges related to their structural integrity and reusability to fully harness their potential. Additionally, MOFs have demonstrated potential for mitigating $PM_{2.5}$ pollution by enhancing filtration efficiency and facilitating photocatalytic degradation. Innovative strategies such as Ag-MOFs@CNF @ZIF-8 and PTZ-1 nanofiber membranes hold great promise in reducing $PM_{2.5}$ levels and toxic gas concentrations while also extending their operational lifespan.

Advanced air purification technologies are essential to combat air pollution caused by the automotive industry. Using MOF-based technologies to lower emissions of nitrogen oxides (NO_x) and volatile organic compounds (VOCs) is one potential approach that has surfaced. MOFs such as NH2-MIL-125 (Ti) and MIL-160 demonstrate impressive adsorption capacity and stability, making them a potential solution to this type of pollution. Additionally, given the growing concerns about climate change, it is crucial to capture and reduce carbon dioxide (CO_2) emissions. MOFs have the potential to optimize CO_2 capture by adjusting pore characteristics and incorporating structural functionalization, hence contributing to global efforts to mitigate CO_2 emissions.

To summarize, MOFs have proven to be adaptable and efficient materials that may be used to treat a wide variety of air contaminants. From capturing harmful gases to reducing fine $PM_{2.5}$ and mitigating CO_2 emissions, the adaptability and multifaceted applications of MOFs underscore their pivotal role in advancing air quality and promoting environmental sustainability.

6.1 Future perspectives

Currently, despite the significant potential of MOFs in adsorbing pollutants, there are still some limitations. For instance, the development of MOFs adsorbents tailored to specific pollutants is at an early stage. The existing methods for preparing and assessing the effectiveness of MOFs are largely confined to laboratory settings, and their performance in real-world applications remains to be thoroughly validated. Furthermore, the adsorption capacity of current MOFs is limited and necessitates replacement upon saturation. Additionally, the production cost of MOFs is relatively high. In the future, with further research and technological advancements, it is anticipated that both the application scope and adsorption capabilities of MOFs will be enhanced. It is recommended that researchers focus on optimizing the pore structure, surface chemistry, and functionalization of MOFs to enhance their pollutant adsorption capacity and selectivity while expanding their applicability. Emphasis should also be placed on developing renewable and biodegradable MOF materials to enable their reuse and minimize environmental impact. Policy makers are encouraged to provide financial support as well as technical assistance to improve essential production infrastructure for these materials. Enterprises should seek closer collaboration with research institutions to facilitate technology transfer for scaled-up production processes and optimization techniques aimed at reducing manufacturing costs. In conclusion, despite facing challenges related to air pollution control efforts; there exists substantial promise for MOFs in safeguarding human health and preserving environmental integrity.

Acknowledgements All the authors thank Prof. Su Shiung Lam and Associate Prof. Shengbo Ge for revising the manuscript. All the authors thank the authorizations for figures from American Chemical Society, Nature Research, Royal Society of Chemistry, Multidisciplinary Digital Publishing Institute, Willy, Nature, Academic Press Inc. Elsevier Science, Elsevier Sci Ltd., Academic Press Inc. Elsevier Science, Elsevier, Elsevier Science SA, and Wiley-VCH Press, respectively.

Author contribution Xiaoyi Duan wrote the main manuscript text. Xiangmeng Chen and Cheng Li prepared all the figures. Erin Witherspoon, Ethan Burcar, Zhe Wang, Aricson Pereira, and Hanyin Li revised the manuscript. Wanxi Peng edited the main manuscript text and supported funding. All authors reviewed the manuscript.

Funding This work was financially supported by the Longzi Lake New Energy Laboratory project (No. LZHLH2023010) and Zhongyuan Scholar Workstation Funding Project (No.224400520013 and No.234400510016).

Data availability The data presented in this study are available on request from the corresponding author.

Declarations

Institutional review board Not applicable.

Informed consent Not applicable.

Conflict of interest The authors declare no competing interests.

References

1. Li X, Jiang Y, Xin X, Nassani AA, Yang C (2024) The asymmetric role of natural resources, fintech and green innovations in the Chinese economy. Evidence from QARDL approach. Res Policy 90:104731. https://doi.org/10.1016/j.resourpol.2024.104731
2. Kulmala M (2015) Atmospheric chemistry: China's choking cocktail. Nature 526:497–499. https://doi.org/10.1038/526497a
3. Xu X, Zhao T, Liu F, Gong SL, Kristovich D, Lu C, Guo Y, Cheng X, Wang Y, Ding G (2016) Climate modulation of the tibetan plateau on haze in china. Atmos Chem Phys 16:3. https://doi.org/10.5194/acp-16-1365-2016
4. Tao M, Chen L, Su L, Tao J (2012) Satellite observation of regional haze pollution over the north china plain. J Geophys Res Atmos 117:D12. https://doi.org/10.1029/2012JD017915
5. Guan WJ, Zheng XY, Chung KF, Zhong NS (2016) Impact of air pollution on the burden of chronic respiratory diseases in China: time for urgent action. Lancet 388:1939–1951. https://doi.org/10.1016/s0140-6736(16)31597-5
6. Chen G, Zhang Y, Zhang W, Li S, Williams G, Marks GB, Jalaludin B, Abramson MJ, Luo F, Yang D (2017) Attributable risks of emergency hospital visits due to air pollutants in China: a multi-city study. Environ Pollut 228:43. https://doi.org/10.1016/j.envpol.2017.05.026
7. Laiguo C, Guocheng H, Ruifang F, Yanshan L, Yanyan D, Zhencheng X (2018) Association of PAHs and BTEX exposure with lung function and respiratory symptoms among a nonoccupational population near the coal chemical industry in Northern China. Environ Int 120:480–488. https://doi.org/10.1016/j.envint.2018.08.004
8. Liu C, Chen R, Zhao Y, Ma Z, Bi J, Liu Y, Meng X, Wang Y, Chen X, Li W (2017) Associations between ambient fine particulate air pollution and hypertension: a nationwide cross-sectional study in china. Sci Total Environ 584-585:869–874. https://doi.org/10.1016/j.scitotenv.2017.01.133
9. Guo P, Feng W, Zheng M, Lv J, Wang L, Liu J, Zhang Y, Luo G, Zhang Y, Deng C (2018) Short-term associations of ambient air pollution and cause-specific emergency department visits in Guangzhou, China. Sci Total Environ 613-614:306–313. https://doi.org/10.1016/j.scitotenv.2017.09.102
10. Ma Y, Yang S, Yu Z, Jiao H, Ma B (2019) A study on the short-term impact of fine particulate matter pollution on the incidence of cardiovascular diseases in Beijing, China. Atmos Environ 215:116889. https://doi.org/10.1016/j.atmosenv.2019.116889
11. Song J, Liu Y, Zheng L, Gui L, Zhao X, Xu D, Wu W (2018) Acute effects of air pollution on type II diabetes mellitus hospitalization in Shijiazhuang, China. Environ Sci Pollut R 25:30151–30159. https://doi.org/10.1007/s11356-018-3016-9
12. Tian L, Qiu H, Sun S, Tsang H, Chan K-P, Leung WK (2017) Association between emergency admission for peptic ulcer bleeding and air pollution: a case-crossover analysis in Hong Kong's elderly population. Lancet Planet Health 1:e74–e81. https://doi.org/10.1016/s2542-5196(17)30021-9
13. Wei Q, Wu J, Zhang Y, Cheng Q, Bai L, Duan J, Gao J, Xu Z, Yi W, Pan R (2019) Short-term exposure to sulfur dioxide and the risk of childhood hand, foot, and mouth disease during different seasons in Hefei, China. Sci Total Environ 658:116–121. https://doi.org/10.1016/j.scitotenv.2018.11.481
14. Heyes A, Zhu M, Cole MA, Lange A, Phaneuf DJ, Popp D, Roberts MJ, Smith MD, Timmins C, Weninger Q (2019) Air pollution as a cause of sleeplessness: social media evidence from a panel of Chinese cities. J Environ Econ Manag 98:102247. https://doi.org/10.1016/j.jeem.2019.07.002
15. Chen C, Liu C, Chen R, Wang W, Fu C (2017) Ambient air pollution and daily hospital admissions for mental disorders in Shanghai, China. Sci Total Environ 613-614:324–330. https://doi.org/10.1016/j.scitotenv.2017.09.098
16. Qiu H, Zhu X, Wang L, Pan J, Pu X, Zeng X, Zhang L, Peng Z, Zhou L (2019) Attributable risk of hospital admissions for overall and specific mental disorders due to particulate matter pollution: a time-series study in Chengdu, China. Environ Res 170:230–237. https://doi.org/10.1016/j.envres.2018.12.019
17. Song J, Liu Y, Lu M, An Z, Lu J, Chao L, Zheng L, Li J, Yao S, Wu W (2019) Short-term exposure to nitrogen dioxide pollution and the risk of eye and adnexa diseases in Xinxiang, China. Atmos Environ 218:117001. https://doi.org/10.1016/j.atmosenv.2019.117001
18. Wang H-H, Zhang S-C, Wang J, Chen X, Yin H, Huang D-Y (2020) Combined toxicity of outdoor air pollution on kidney function among adult women in Mianyang city, southwest China. Chemosphere 238:124603. https://doi.org/10.1016/j.chemosphere.2019.124603
19. Chen SY, Chu DC, Lee JH, Yang YR, Chan CC (2018) Traffic-related air pollution associated with chronic kidney disease among elderly residents in Taipei city. Environ Pollut 234:838–845. https://doi.org/10.1016/j.envpol.2017.11.084
20. Lin H, Liang Z, Liu T, Di Q, Qian Z, Zeng W, Xiao J, Li X, Guo L, Ma W (2015) Association between exposure to ambient air pollution before conception date and likelihood of giving birth to girls in Guangzhou, China. Atmos Environ 122:622–627. https://doi.org/10.1016/j.atmosenv.2015.10.035
21. Han Y, Jiang P, Dong T, Ding X, Chen T, Villanger GD, Aase H, Huang L, Xia Y (2018) Maternal air pollution exposure and preterm birth in Wuxi, China: effect modification by maternal age. Ecotox Environ Safe 157:457–462. https://doi.org/10.1016/j.ecoenv.2018.04.002
22. Liu H, Liao J, Jiang Y, Zhang B, Yu H, Kang J, Hu C, Li Y, Xu S (2019) Maternal exposure to fine particulate matter and the risk of fetal distress. Ecotox Environ Safe 170:253–258. https://doi.org/10.1016/j.ecoenv.2018.11.068
23. González-Díaz SN, Arias-Cruz A, Macouzet-Sánchez C, Partida-Ortega AB (2016) Partida-Ortega. Impact of air pollution in respiratory allergic diseases. Medicina Universitaria 18:212–215. https://doi.org/10.1016/j.rmu.2016.10.006
24. Zhang M, Sun X, Wang W (2020) Study on the effect of environmental regulations and industrial structure on haze pollution in China from the dual perspective of independence and linkage. J Clean Prod 256:120748. https://doi.org/10.1016/j.jclepro.2020.120748
25. Rehdanz K, Maddison D (2008) Local environmental quality and life-satisfaction in Germany. Ecol Econ 64:787–797. https://doi.org/10.1016/j.ecolecon.2007.04.016
26. Liu J, Zhang S, Wagner F (2018) Exploring the driving forces of energy consumption and environmental pollution in China's cement industry at the provincial level. J Clean Prod 184:274–285. https://doi.org/10.1016/j.jclepro.2018.02.277
27. Song Y, Zhou A, Zhang M, Wang H (2019) Assessing the effects of haze pollution on subjective well-being based on Chinese general social survey. J Clean Prod 235:574–582. https://doi.org/10.1016/j.jclepro.2019.07.021
28. Zhao C, Deng M, Cao X (2021) Does haze pollution damage urban innovation? Empirical evidence from China. Environ Sci Pollut R 28:16334–16349. https://doi.org/10.1007/s11356-020-11874-x
29. Dong D, Xu X, Xu W, Xie J (2019) The relationship between the actual level of air pollution and residents' concern about air pollution: evidence from shanghai, china. Int J Env Res Pub He 16:4784. https://doi.org/10.3390/ijerph16234784
30. Lelieveld J, Evans JS, Fnais M, Giannadaki D, Pozzer A (2015) The contribution of outdoor air pollution sources to premature

mortality on a global scale. Nature 525:367–371. https://doi.org/10.1038/nature15371
31. Cheng Y, Zheng G, Wei C, Mu Q, Zheng B, Wang Z, Gao M, Zhang Q, He K, Carmichael G (2016) Reactive nitrogen chemistry in aerosol water as a source of sulfate during haze events in China. Sci Adv 2:e1601530. https://doi.org/10.1126/sciadv.1601530
32. Guo S, Hu M, Zamora ML, Peng J, Shang D, Zheng J, Du Z, Wu Z, Shao M, Zeng L (2014) Elucidating severe urban haze formation in China. P Natl Acad Sci Usa 111:17373–17378. https://doi.org/10.1073/pnas.1419604111
33. Fortner EC, Zheng J, Zhang R, Berk Knighton W, Volkamer RM, Sheehy P, Molina L, André M (2009) Measurements of volatile organic compounds using proton transfer reaction – mass spectrometry during the MILAGRO 2006 campaign. Atmos Chem Phys 9:467–481. https://doi.org/10.5194/acp-9-467-2009
34. Wang M, Zhu T, Zheng J, Zhang RY, Zhang SQ, Xie XX, Han YQ, Li Y (2009) Use of a mobile laboratory to evaluate changes in on-road air pollutants during the Beijing 2008 Summer Olympics. Atmos Chem Phys 9:8247–8263. https://doi.org/10.5194/acp-9-8247-2009
35. Zhao J, Zhang R, Misawa K, Shibuya K (2005) Experimental product study of the oh-initiated oxidation of m-xylene. J Photoch Photobio A 176:199–207. https://doi.org/10.1016/j.jphotochem.2005.07.013
36. Chen L, Shi M, Li S, Gao S, Zhang H, Sun Y, Mao J, Bai Z, Wang Z, Zhou J (2017) Quantifying public health benefits of environmental strategy of $PM_{2.5}$ air quality management in Beijing–Tianjin–Hebei region, China. J Environ Sci 57:33–40. https://doi.org/10.1016/j.jes.2016.11.014
37. Song C, He J, Wu L, Jin T, Chen X, Li R, Ren P, Zhang L, Mao H (2017) Health burden attributable to ambient $PM_{2.5}$ in China. Environ Pollut 223:575–586. https://doi.org/10.1016/j.envpol.2017.01.060
38. Li B, Wang J, Nassani AA, Binsaeed RH, Li Z (2023) The future of green energy: a panel study on the role of renewable resources in the transition to a green economy. Energy Econ 127:107026. https://doi.org/10.1016/j.eneco.2023.107026
39. Zhiming L, Jiming H, Lixin F, Junhua L, Xiangyu C (2004) Advances in catalytic removal of NO_x under lean-burn conditions. Chin Sci Bull 49:2231–2241. https://doi.org/10.1360/04wb0054
40. Li J, Hao J, Cui X, Fu L (2005) Influence of preparation methods of In_2O_3/Al_2O_3 catalyst on selective catalytic reduction of no by propene in the presence of oxygen. Catal Lett 103:75–82. https://doi.org/10.1007/s10562-005-6506-6
41. Wang X, Li Y (2016) Nanoporous carbons derived from MOFs as metal-free catalysts for selective aerobic oxidations. J Mater Chem A 4:5247–5257. https://doi.org/10.1039/C6TA00324A
42. Wang M, Zhang J, Yi X, Zhao X, Liu X (2019) Nitrogen-doped hierarchical porous carbon derived from ZIF-8 supported on carbon aerogels with advanced performance for supercapacitor. Appl Surf Sci 507:145166. https://doi.org/10.1016/j.apsusc.2019.145166
43. Zhang Y, Wang P, Yang J, Lu S, Qiu J (2021) Decorating ZIF-67-derived cobalt-nitrogen doped carbon nanocapsules on 3D carbon frameworks for efficient oxygen reduction and oxygen evolution. Carbon 177:344–356. https://doi.org/10.1016/j.carbon.2021.02.052
44. Li J, Yan D, Zhang X et al (2017) ZnS nanoparticles decorated on nitrogen-doped porous carbon polyhedra: a promising anode material for lithium-ion and sodium-ion batteries. J Mater Chem A 5:20428–20438. https://doi.org/10.1039/C7TA06180C
45. Tan K, Zuluaga S, Wang H, Canepa P, Soliman K, Cure J, Li J, Thonhauser T, Chabal YJ (2017) Interaction of acid gases SO_2 and NO_2 with coordinatively unsaturated metal organic frameworks: M-MOF-74 (M = Zn, Mg, Ni, Co). Chem Mater 29:4227–4235. https://doi.org/10.1021/acs.chemmater.7b00005
46. Yang S, Sun J, Ramirez-Cuesta AJ, Callear SK, David WI, Anderson DP, Newby R, Blake AJ, Parker JE, Tang CC (2012) Selectivity and direct visualization of carbon dioxide and sulfur dioxide in a decorated porous host. Nat Chem 4:887–894. https://doi.org/10.1038/nchem.1457
47. Carter JH, Han X, Moreau FY, Da Silva I, Nevin A, Godfrey HG, Tang CC, Yang S, Schröder M (2018) Exceptional adsorption and binding of sulfur dioxide in a robust zirconium-based metal–organic framework. J Am Chem Soc 140:15564–15567. https://doi.org/10.1021/jacs.8b08433
48. DMello ME, Sundaram NG, Singh A, Singh AK, Kalidindi SB (2019) An amine functionalized zirconium metal–organic framework as an effective chemiresistive sensor for acidic gases. Chem Commun 55:349–352. https://doi.org/10.1039/C8CC06875E
49. Rowsell JL, Yaghi OM (2005) Strategies for hydrogen storage in metal–organic frameworks. Angew Chem Int Edit 44:4670–4679. https://doi.org/10.1002/anie.200462786
50. Sohail M, Yun Y-N, Lee E, Kim SK, Cho K, Kim J-N, Kim TW, Moon J-H, Kim H (2017) Synthesis of highly crystalline NH2-MIL-125 (Ti) with s-shaped water isotherms for adsorption heat transformation. Cryst Growth Des 17:1208–1213. https://doi.org/10.1021/acs.cgd.6b01597
51. Brandt P, Nuhnen A, Lange M, Möllmer J, Weingart O, Janiak C (2019) Metal–organic frameworks with potential application for SO_2 separation and flue gas desulfurization. ACS Appl Mater Interfaces 11:17350–17358. https://doi.org/10.1021/acsami.9b00029
52. Ebrahim AM, Levasseur B, Bandosz TJ (2013) Interactions of NO_2 with Zr-based MOF: effects of the size of organic linkers on NO_2 adsorption at ambient conditions. Langmuir 29:168–174. https://doi.org/10.1021/la302869m
53. Sharma D, Rasaily S, Pradhan S, Baruah K, Tamang S, Pariyar A (2021) HKUST-1 metal organic framework as an efficient dual-function catalyst: aziridination and one-pot ring-opening transformation for formation of β-aryl sulfonamides with C–C, C–N, C–S, and C–O bonds. Inorg Chem 60:7794–7802. https://doi.org/10.1021/acs.inorgchem.1c00201
54. Cattaneo D, Warrender SJ, Duncan MJ, Kelsall CJ, Doherty MK, Whitfield PD, Megson IL, Morris RE (2016) Tuning the nitric oxide release from CPO-27 MOFs. RSC Adv 6:14059–14067. https://doi.org/10.1039/C5RA24023A
55. Brozek CK, Miller JT, Stoian SA, Dincă M (2015) NO disproportionation at a mononuclear site-isolated Fe^{2+} center in Fe^{2+}-MOF-5. J Am Chem Soc 137:7495–7501. https://doi.org/10.1021/jacs.5b03761
56. Schulz M, Gehl A, Schlenkrich J, Schulze HA, Zimmermann S, Schaate A (2018) A calixarene-based metal–organic framework for highly selective NO_2 detection. Angew Chem Int Edit 57:12961–12965. https://doi.org/10.1002/anie.201805355
57. Han X, Godfrey HG, Briggs L, Davies AJ, Cheng Y, Daemen LL, Sheveleva AM, Tuna F, McInnes EJ, Sun J (2018) Reversible adsorption of nitrogen dioxide within a robust porous metal–organic framework. Nat Mater 17:691–696. https://doi.org/10.1038/s41563-018-0104-7
58. Zhang J, Li P, Zhang X, Ma X, Wang B (2020) Aluminum metal-organic frameworks with photocatalytic antibacterial activity for autonomous indoor humidity control. ACS Appl Mater Interfaces 12. https://doi.org/10.1021/acsami.0c12693
59. Ma D, Li P, Duan X, Li J, Shao P, Lang Z, Bao L, Zhang Y, Lin Z, Wang B (2020) A hydrolytically stable vanadium (iv) metal–organic framework with photocatalytic bacteriostatic activity for autonomous indoor humidity control. Angew Chem 132:3933–3937. https://doi.org/10.1002/anie.201914762

60. Li P, Li J, Feng X, Li J, Hao Y, Zhang J, Wang H, Yin A, Zhou J, Ma X (2019) Metal-organic frameworks with photocatalytic bactericidal activity for integrated air cleaning. Nat Commun 10:2177. https://doi.org/10.1038/s41467-019-10218-9
61. Lin S, Liu X, Tan L, Cui Z, Yang X, Yeung KW, Pan H, Wu S (2017) Porous iron-carboxylate metal–organic framework: a novel bioplatform with sustained antibacterial efficacy and nontoxicity. ACS Appl Mater Interfaces 9:19248–19257. https://doi.org/10.1021/acsami.7b04810
62. Zhang Y, He X, Zhu Z, Wang W-N, Chen S-C (2021) Simultaneous removal of vocs and $PM_{2.5}$ by metal-organic framework coated electret filter media. J Membr Sci 618:118629. https://doi.org/10.1016/j.memsci.2020.118629
63. Jeremias F, Khutia A, Henninger SK, Janiak C (2012) MIL-100(Al, Fe) as water adsorbents for heat transformation purposes—a promising application. J Mater Chem 22:10148–10151. https://doi.org/10.1039/C2JM15615F
64. Ehrenmann J, Henninger SK, Janiak C (2011) Water adsorption characteristics of MIL-101 for heat-transformation applications of MOFs. Eur J Inorg Chem 2011:471–474. https://doi.org/10.1002/ejic.201001156
65. Chen Y-J, Chen Y, Miao C, Wang YR, Gao GK, Yang RX, Zhu H-J, Wang J-H, Li S, Lan Y (2020) Metal–organic framework-based foams for efficient microplastics removal. J Mater Chem 8:14644–14652. https://doi.org/10.1039/D0TA04891G
66. Wan H, Wang J, Sheng X, Yan J, Zhang W, Xu Y (2022) Removal of polystyrene microplastics from aqueous solution using the metal-organic framework material of ZIF-67. Toxics 10:70. https://doi.org/10.3390/toxics10020070
67. Yang Z, Zhen Y, Feng Y, Jiang X, Qin Z, Yang W, Qie Y (2022) Polyacrylonitrile@TiO_2 nanofibrous membrane decorated by MOF for efficient filtration and green degradation of $PM_{2.5}$. J Colloid Interface Sci 635:598–610. https://doi.org/10.1016/j.jcis.2022.12.122
68. Wu S, Ren D, Zhou K, Xia HL, Li J (2021) Linker engineering toward full-color emission of UiO-68 type metal-organic frameworks. J Am Chem Soc 143:10547–10552. https://doi.org/10.1021/jacs.1c04810
69. Ma S, Zhang M, Nie J, Tan J, Yang B, Song S (2019) Design of double-component metal-organic framework air filters with $PM_{2.5}$ capture, gas adsorption and antibacterial capacities. Carbohydr Polym 203:415–422. https://doi.org/10.1016/j.carbpol.2018.09.039
70. Huang Q, Hu Y, Pei Y, Zhang J, Fu M (2019) In situ synthesis of TiO_2@NH_2-MIL-125 composites for use in combined adsorption and photocatalytic degradation of formaldehyde. Appl Catal B-Environ 259:118106. https://doi.org/10.1016/j.apcatb.2019.118106
71. Zhang ZF, Mingli (2020) TiO_2-UiO-66-NH_2 nanocomposites as efficient photocatalysts for the oxidation of VOCs. Chem Eng J 385:123814. https://doi.org/10.1016/j.cej.2019.123814
72. Pellegrino F, Zangirolami M, Minero C, Maurino V (2020) Portable photoreactor for on-site measurement of the activity of photocatalytic surfaces. Catal Today 340:363–368. https://doi.org/10.1016/j.cattod.2018.09.023
73. Brattich E, Barbano F, Pulvirenti B, Pilla F, Bacchetti M, Sabatino SD (2021) The effect of photocatalytic coatings on NO_x concentrations in real-world street canyons. Build Environ 205:108312. https://doi.org/10.1016/j.buildenv.2021.108312
74. Debono O, Hequet V, Coq LL, Locoge N, Thevenet F (2017) VOC mixture effect on ppb level photocatalytic oxidation: removal kinetic, reaction intermediates and mineralization. Appl Catal B-Environ 218. https://doi.org/10.1016/j.apcatb.2017.06.070
75. F. Gorky, A. Nambo, M. L. Carreon (2021) Cold plasma-Metal Organic Framework (MOF)-177 breathable system for atmospheric remediation. J Co_2 Util 51: 101642. https://doi.org/10.1016/J.JCOU.2021.101642
76. Darunte LA, Oetomo AD, Walton KS, Sholl DS, Jones CW (2016) Direct air capture of CO_2 using amine functionalized MIL-101 (Cr). ACS Sustain Chem Eng 4:5761–5768. https://doi.org/10.1021/acssuschemeng.6b01692
77. Ben-Mansour R, Qasem NAA (2018) An efficient temperature swing adsorption (TSA) process for separating CO_2 from CO_2/N_2 mixture using Mg-MOF-74. Energ Convers Manage 156:10–24. https://doi.org/10.1016/j.enconman.2017.11.010
78. Zhang X, Sun J, Wei G, Liu Z, Yang H, Wang K, Fei H (2019) In situ generation of an N-heterocyclic carbene functionalized metal–organic framework by postsynthetic ligand exchange: efficient and selective hydrosilylation of CO_2. Angew Chem Int Edit 58:2844–2849. https://doi.org/10.1002/anie.201813064
79. Glover TG, Peterson GW, Schindler BJ, Britt D, Yaghi O (2011) MOF-74 building unit has a direct impact on toxic gas adsorption. Chem Eng Sci 66:163–170. https://doi.org/10.1016/j.ces.2010.10.002
80. Hamon L, Serre C, Devic T, Loiseau T, Millange F, Ferey GR, Weireld GD (2009) Comparative study of hydrogen sulfide adsorption in the MIL-53(Al, Cr, Fe), MIL-47(V), MIL -100(Cr), and MIL-101(Cr) metalorganic frameworks at room temperature. J Am Chem Soc 131:8775–8777. https://doi.org/10.1021/ja901587t
81. Zhang Z, Huang Y, Ding W, Li G (2014) Multilayer interparticle linking hybrid MOF-199 for noninvasive enrichment and analysis of plant hormone ethylene. Anal Chem 86:3533–3540. https://doi.org/10.1021/ac404240n
82. Amoatey P, Omidvarborna H, Baawain MS, Al-Mamun A (2019) Emissions and exposure assessments of SO_x, NO_x, $PM_{10/2.5}$ and trace metals from oil industries: a review study (2000–2018). Process Saf Environ 123:215–228. https://doi.org/10.1016/j.psep.2019.01.014
83. Su Z, Zhang M, Lu Z, Song S, Zhao Y, Hao Y (2018) Functionalization of cellulose fiber by in situ growth of zeolitic imidazolate framework-8 (ZIF-8) nanocrystals for preparing a cellulose-based air filter with gas adsorption ability. Cellulose 25:1997–2008. https://doi.org/10.1007/s10570-018-1696-4
84. Lu W, Wei Z, Gu Z-Y, Liu T-F, Park J, Park J, Tian J, Zhang M, Zhang Q, Gentle T III (2014) Tuning the structure and function of metal–organic frameworks via linker design. Chem Soc Rev 43:5561–5593. https://doi.org/10.1039/C4CS00003J
85. Mendes RF, Paz FAA (2015) Transforming metal–organic frameworks into functional materials. Inorg Chem Front 2:495–509. https://doi.org/10.1039/C4QI00222A
86. Li N, Xu J, Feng R, Hu T-L, Bu X-H (2016) Governing metal–organic frameworks towards high stability. Chem Commun 52:8501–8513. https://doi.org/10.1039/C6CC02931K
87. Gao S, Zhao N, Shu M, Che S (2010) Palladium nanoparticles supported on MOF-5: a highly active catalyst for a ligand-and copper-free Sonogashira coupling reaction. Appl Catal A-Gen 388:196–201. https://doi.org/10.1016/J.APCATA.2010.08.045
88. Bobbitt NS, Mendonca ML, Howarth AJ, Islamoglu T, Hupp JT, Farha OK, Snurr RQ (2017) Metal–organic frameworks for the removal of toxic industrial chemicals and chemical warfare agents. Chem Soc Rev 46:3357–3385. https://doi.org/10.1039/C7CS00108H
89. Rosi NL, Kim J, Eddaoudi M, Chen B, O'Keeffe M, Yaghi OM (2005) Rod packings and metal−organic frameworks constructed from rod-shaped secondary building units. J Am Chem Soc 127:1504–1518. https://doi.org/10.1021/ja045123o
90. Islamoglu T, Chen Z, Wasson MC, Buru CT, Kirlikovali KO, Afrin U, Mian MR, Farha OK (2020) Metal–organic frameworks against toxic chemicals. Chem Rev 120:8130–8160. https://doi.org/10.1021/acs.chemrev.9b00828

91. Sun W, Lin LC, Peng X, Smit B (2014) Computational screening of porous metal-organic frameworks and zeolites for the removal of SO_2 and NO_x from flue gases. AICHE J 60:2314–2323. https://doi.org/10.1002/aic.14467
92. Guo D, Li H, Xu Z, Nie Y (2023) Development of pyrene-based MOFs probe for water content and investigations on their mechanochromism and acidochromism. J Alloys Compd 968:172004. https://doi.org/10.1016/j.jallcom.2023.172004
93. Chernikova V, Yassine O, Shekhah O, Eddaoudi M, Salama KN (2018) Highly sensitive and selective SO_2 MOF sensor: the integration of MFM-300 MOF as a sensitive layer on a capacitive interdigitated electrode. J Mater Chem A 6:5550–5554. https://doi.org/10.1039/C7TA10538J
94. Granger P, Pârvulescu V (2007) Past and present in DeNOx catalysis: from molecular modelling to chemical engineering. Elsevier, p 171. https://doi.org/10.1016/S1351-4180(08)70386-6
95. Zhang WJ, Bagreev R, Rasouli F (2008) Reaction of NO_2 with activated carbon at ambient temperature. Ind Eng Chem Res 47:4358–4362. https://doi.org/10.1021/ie800249s
96. Han X et al (2020) Adsorption of nitrogen dioxide in a redox-active vanadium metal–organic framework material. J Am Chem Soc 142:15235–15239. https://doi.org/10.1021/jacs.0c06414
97. Petit C, Mendoza B, Bandosz TJ (2010) Reactive adsorption of ammonia on Cu-based MOF/graphene composites. Langmuir 26:15302–15309. https://doi.org/10.1021/la1021092
98. Petit C, Levasseur B, Mendoza B, Bandosz TJ (2012) Reactive adsorption of acidic gases on MOF/graphite oxide composites. Microporous Mesoporous Mater 154:107–112. https://doi.org/10.1016/j.micromeso.2011.09.012
99. Mavrandonakis A, Klontzas E, Tylianakis E, Froudakis GE (2009) Enhancement of hydrogen adsorption in metal-organic frameworks by the incorporation of the sulfonate group and Li cations. A multiscale computational study. J Am Chem Soc 131:13410–13414. https://doi.org/10.1021/ja9043888
100. Zong S, Huang S, Shi X-R, Sun C, Xu S, Ma P, Wang J (2020) Impact of linker functionalization on the adsorption of nitrogen-containing compounds in HKUST-1. Dalton T 49:12610–12621. https://doi.org/10.1039/D0DT02165B
101. Jagódka P, Matus K, Łamacz A (2022) On the HKUST-1/GO and HKUST-1/rGO composites: the impact of synthesis method on physicochemical properties. Molecules 27:7082. https://doi.org/10.3390/molecules27207082
102. Levasseur B, Petit C, Bandosz TJ (2010) Reactive adsorption of NO_2 on copper-based metal-organic framework and graphite oxide/ metal-organic Framework composites. ACS Appl Mater Interfaces 2:3606–3613. https://doi.org/10.1021/am100790v
103. Peterson GW, Mahle JJ, DeCoste JB, Gordon WO, Rossin JA (2016) Extraordinary NO_2 removal by the metal–organic framework UiO-66-NH_2. Angew Chem 128:6343–6346. https://doi.org/10.1002/anie.201601782
104. McGrath DT, Ryan MD, MacInnis JJ, VandenBoer TC, Young CJ, Katz MJ (2019) Selective decontamination of the reactive air pollutant nitrous acid via node-linker cooperativity in a metal–organic framework. Chem Sci 10:5576–5581. https://doi.org/10.1039/C9SC01357A
105. Xiao B, Wheatley PS, Zhao X, Fletcher AJ, Fox S, Rossi AG, Megson IL, Bordiga S, Regli L, Thomas KM (2007) High-capacity hydrogen and nitric oxide adsorption and storage in a metal-organic framework. J Am Chem Soc 129:1203–1209. https://doi.org/10.1021/ja066098k
106. Petäjä T, Järvi L, Kerminen V-M, Ding A, Sun J, Nie W, Kujansuu J, Virkkula A, Yang X, Fu C (2016) Enhanced air pollution via aerosol-boundary layer feedback in China. Sci Rep-Uk 6:18998. https://doi.org/10.1038/srep18998
107. Zhu Z, Zhang Y, Bao L, Chen J, Duan S, Chen S-C, Xu P, Wang W-N (2021) Self-decontaminating nanofibrous filters for efficient particulate matter removal and airborne bacteria inactivation. Environ Sci-Nano 8:1081–1095. https://doi.org/10.1039/D0EN01230K
108. Wan H, Wang N, Yang J, Si Y, Chen K, Ding B, Sun G, El-Newehy M, Al-Deyab SS, Yu J (2014) Hierarchically structured polysulfone/titania fibrous membranes with enhanced air filtration performance. J Colloid Interface Sci 417:18–26. https://doi.org/10.1016/j.jcis.2013.11.009
109. Zuo F, Zhang S, Liu H, Fong H, Yin X, Yu J, Ding B (2017) Free-standing polyurethane nanofiber/nets air filters for effective pm capture. Small 13:1702139. https://doi.org/10.1002/smll.201702139
110. Souzandeh H, Wang Y, Zhong W-H (2016) "Green" nanofilters: fine nanofibers of natural protein for high efficiency filtration of particulate pollutants and toxic gases. RSC Adv 6:105948–105956. https://doi.org/10.1039/C6RA24512A
111. Yoon Y, Kim S, Ahn KH, Ko KB, Kim K-S (2016) Fabrication and characterization of micro-porous cellulose filters for indoor air quality control. Environ Technol 37:703–712. https://doi.org/10.1080/09593330.2015.1078416
112. Guo J, Hanif A, Shang J, Deka BJ, Zhi N, An AK (2021) Paa@ZIF-8 incorporated nanofibrous membrane for high-efficiency $PM_{2.5}$ capture. Chem Eng J 405:126584. https://doi.org/10.1016/j.cej.2020.126584
113. Zhang Y, Zhu Z, Wang W-N, Chen S-C (2023) A novel sustainable semiconductor/metal-organic framework coated electret filter for simultaneous removal of $PM_{2.5}$ and VOCs. Aerosol Air Qual Res 23:220445. https://doi.org/10.4209/aaqr.220445
114. Schreck M, Niederberger M (2019) Photocatalytic gas phase reactions. Chem Mater 31:597–618. https://doi.org/10.1021/ACS.CHEMMATER.8B04444
115. Fujisima A, Honda K (1972) Photolysis-decomposition of water at surface of an irradiated semiconduction. Nature 238:37–38. https://doi.org/10.1038/238238a0
116. Vickers NJ (2017) Animal communication: when I'm calling you, will you answer too? Curr Biol 27:R713–R715. https://doi.org/10.1016/j.cub.2017.05.064
117. Zhu Z, Bao L, Pestov D, Xu P, Wang W-N (2023) Cellular-level insight into biointerface: from surface charge modulation to boosted photocatalytic oxidative disinfection. Chem Eng J 453:139956. https://doi.org/10.1016/j.cej.2022.139956
118. Li T-T, Cen X, Ren H-T, Wu L, Peng H-K, Wang W, Gao B, Lou C-W, Lin J-H (2020) Zeolitic imidazolate framework-8/polypropylene–polycarbonate barklike meltblown fibrous membranes by a facile in situ growth method for efficient $PM_{2.5}$ capture. ACS Appl Mater Interfaces 12:8730–8739. https://doi.org/10.1021/acsami.9b21340
119. Chen Y, Zhang S, Cao S, Li S, Chen F, Yuan S, Xu C, Zhou J, Feng X, Ma X (2017) Roll-to-roll production of metal-organic framework coatings for particulate matter removal. Adv Mater 29:1606221. https://doi.org/10.1002/adma.201606221
120. Zhang S, Liu H, Yin X, Yu J, Ding B (2016) Anti-deformed polyacrylonitrile/polysulfone composite membrane with binary structures for effective air filtration. ACS Appl Mater Interfaces 8:8086–8095. https://doi.org/10.1021/acsami.6b00359
121. Qian L, Lei D, Duan X, Zhang S, Song W, Hou C, Tang R (2018) Design and preparation of metal-organic framework papers with enhanced mechanical properties and good antibacterial capacity. Carbohydr Polym 192:44–51. https://doi.org/10.1016/j.carbpol.2018.03.049
122. Russell BA, Migone AD (2017) Low temperature adsorption study of CO_2 in ZIF-8. Microporous Mesoporous Mater 246:178–185. https://doi.org/10.1016/j.micromeso.2017.03.030
123. Zhang Y, Yuan S, Feng X, Li H, Zhou J, Wang B (2016) Preparation of nanofibrous metal–organic framework filters for efficient

air pollution control. J Am Chem Soc 138:5785–5788. https://doi.org/10.1021/jacs.6b02553
124. Schultz AA, Schauer JJ, Malecki KM (2017) Allergic disease associations with regional and localized estimates of air pollution. Environ Res 155:77–85. https://doi.org/10.1016/j.envres.2017.01.039
125. Lyu W, Hu Y, Liu J, Deng J et al (2024) Impact of battery electric vehicle usage on air quality in three Chinese first-tier cities. Sci Rep-Uk 14:21. https://doi.org/10.1038/s41598-023-50745-6
126. Zhao J, Sun J, Meng X, Li Z (2022) Recent advances in vehicle exhaust treatment with photocatalytic technology. Catalysts 12:1051. https://doi.org/10.3390/catal12091051
127. Suwannasual U, Lucero JA, Mcdonald JD, Lund AK (2017) Exposure to traffic-generated air pollutants mediates alterations in brain microvascular integrity in wildtype mice on a high-fat diet. Environ Res 160:449–461. https://doi.org/10.1016/j.envres.2017.10.029
128. Zhang Y, Deng W, Hu Q, Wu Z, Yang W, Zhang H, Wang Z, Fang Z, Zhu M, Li S (2020) Comparison between idling and cruising gasoline vehicles in primary emissions and secondary organic aerosol formation during photochemical ageing. Sci Total Environ 722:137934. https://doi.org/10.1016/j.scitotenv.2020.137934
129. Gholami F, Tomas M, Gholami Z, Vakili M (2020) Technologies for the nitrogen oxides reduction from flue gas: a review. Sci Total Environ 714:136712. https://doi.org/10.1016/j.scitotenv.2020.136712
130. Liu Z, Yu F, Ma C, Dan J, Luo J, Dai B (2019) A critical review of recent progress and perspective in practical denitration application. Catalysts 9:771. https://doi.org/10.3390/catal9090771
131. Pignattelli S, Broccoli A, Piccardo M, Terlizzi A, Renzi M (2021) Effects of polyethylene terephthalate (pet) microplastics and acid rain on physiology and growth of lepidium sativum. Environ Pollut 282:116997. https://doi.org/10.1016/j.envpol.2021.116997
132. Marinos RE, Campbell JL, Driscoll CT, Likens GE, McDowell WH, Rosi EJ, Rustad LE, Bernhardt ES (2018) Give and take: a watershed acid rain mitigation experiment increases baseflow nitrogen retention but increases stormflow nitrogen export. Environ Sci Technol 52:13155–13165. https://doi.org/10.1021/acs.est.8b03553
133. Feng X, Liu Q, Wang S, Cen L, Li H (2021) Arsenopyrite weathering in acid rain: arsenic transfer and environmental implications. J Hazard Mater 420:126612. https://doi.org/10.1016/j.jhazmat.2021.126612
134. Schirmer WN, Olanyk LZ, Guedes CLB, Quessada TP, Ribeiro CB, Capanema MA (2017) Effects of air/fuel ratio on gas emissions in a small spark-ignited non-road engine operating with different gasoline/ethanol blends. Environ Sci Pollut R 24:20354–20359. https://doi.org/10.1007/s11356-017-9651-8
135. McGee Hargrove M, Snow SJ, Luebke RW, Wood CE, Krug JD, Krantz QT, King C, Copeland CB, McCullough SD, Gowdy KM (2018) Effects of simulated smog atmospheres in rodent models of metabolic and immunologic dysfunction. Environ Sci Technol 52:3062–3070. https://doi.org/10.1021/acs.est.7b06534
136. Ali Y, Razi M, De Felice F, Sabir M, Petrillo A (2019) A VIKOR based approach for assessing the social, environmental and economic effects of "smog" on human health. Sci Total Environ 650:2897–2905. https://doi.org/10.1016/j.scitotenv.2018.10.041
137. Lambert CK (2019) Current state of the art and future needs for automotive exhaust catalysis. Nat Catal 2:554–557. https://doi.org/10.1038/s41929-019-0303-x
138. Gandhi H, Graham G, McCabe RW (2003) Automotive exhaust catalysis. J Catal 216:433–442. https://doi.org/10.1016/S0021-9517(02)00067-2
139. Shelef M, Graham G (1994) Why rhodium in automotive three-way catalysts? Catal Rev 36:433–457
140. Farrauto RJ, Deeba M, Alerasool S (2019) Gasoline automobile catalysis and its historical journey to cleaner air. Nat Catal 2:603–613. https://doi.org/10.1038/s41929-019-0312-9
141. Poulakis E, Philippopoulos C (2017) Photocatalytic treatment of automotive exhaust emissions. Chem Eng J 309:178–186. https://doi.org/10.1016/j.cej.2016.10.030
142. Sun Z, Liao Y, Zhao S et al (2022) Research progress in metal–organic frameworks (MOFs) in CO 2 capture from post-combustion coal-fired flue gas: characteristics, preparation, modification and applications. J Mater Chem A 10:5174–5211. https://doi.org/10.1039/D1TA07856A
143. Jansson I, Kobayashi K, Hori H et al (2016) Decahedral anatase titania particles immobilized on zeolitic materials for photocatalytic degradation of VOC. Catal Today 287:22–29. https://doi.org/10.1016/j.cattod.2016.11.041
144. Debono O, Gaudion V, Redon N, Locoge N, Thevenet F (2018) Photocatalytic treatment of VOC industrial emissions: IPA removal using a sensor-instrumented reactor. Chem Eng J 353:394–409. https://doi.org/10.1016/j.cej.2018.07.151
145. Gao X, Huang K, Zhang Z, Meng X (2022) Bismuth chromate ($Cr_2Bi_3O_{11}$): a new bismuth-based semiconductor with excellent photocatalytic activity. Chem Commun 58:2014–2017. https://doi.org/10.1039/D1CC06734F
146. Lu G, Chu F, Huang X, Li Y, Liang K, Wang G (2022) Recent advances in metal-organic frameworks-based materials for photocatalytic selective oxidation. Coord Chem Rev 450:214240. https://doi.org/10.1016/j.ccr.2021.214240
147. Krishnamurthy A, Adebayo B, Gelles T, Rownaghi A, Rezaei F (2019) Abatement of gaseous volatile organic compounds: a process perspective. Catal Today 350:100–119. https://doi.org/10.1016/j.cattod.2019.05.069
148. Liu L, Zhang L, Wang F, Qi K, Zhang H, Cui X, Zheng W (2019) Bi-metal–organic frameworks type II heterostructures for enhanced photocatalytic styrene oxidation. Nanoscale 11:7554–7559. https://doi.org/10.1039/C9NR00790C
149. Zhang Z, Li X, Liu B, Zhao Q, Chen G (2016) Hexagonal microspindle of NH_2-MIL-101 (Fe) metal–organic frameworks with visible-light-induced photocatalytic activity for the degradation of toluene. RSC Adv 6:4289–4295
150. Mahy JG, Paez CA, Hollevoet J, Courard L, Boonen E, Lambert SD (2019) Durable photocatalytic thin coatings for road applications. Constr Build Mater 215:422–434. https://doi.org/10.1016/j.conbuildmat.2019.04.222
151. Ma Y, Li L, Wang H, Wang W, Zheng K (2021) Laboratory study on performance evaluation and automobile exhaust degradation of nano-TiO_2 particles-modified asphalt materials. Adv Mater Sci Eng 2021:1–13. https://doi.org/10.1155/2021/5574013
152. Liu MY, Yang ZY, Dai WK, Huang JQ, Li YH, Zhang J, Qiu CZ, Wei C, Zhou Q, Sun X (2017) Protective effect of Bifidobacterium infantis CGMCC313-2 on ovalbumin-induced airway asthma and β-lactoglobulin-induced intestinal food allergy mouse models. World J Gastroenterol 23:2149–2158. https://doi.org/10.3748/wjg.v23.i12.2149
153. Singh H, Thind PS, Singh S, John S (2022) Applicability of TiO_2-laden asphalt pavements in reducing the vehicular pollution of Chandigarh, India. Clean-Soil Air Water 50:2000461. https://doi.org/10.1002/clen.202000461
154. Wang D, Leng Z, Hueben M, Oeser M, Steinauer B (2016) Photocatalytic pavements with epoxy-bonded TiO_2-containing spreading material. Constr Build Mater 107:44–51. https://doi.org/10.1016/j.conbuildmat.2015.12.164
155. Cui Y, Su W, Xing Y et al (2023) Experimental and simulation evaluation of CO2/CO separation under different component ratios in blast furnace gas on zeolites. Chem Eng J 472:144579. https://doi.org/10.1016/j.cej.2023.144579

156. Ghanbari T, Abnisa F, Daud WMAW (2020) A review on production of metal organic frameworks (MOF) for CO_2 adsorption. Sci Total Environ 707:135090
157. Li H, Hill MR (2017) Low-energy CO_2 release from metal–organic frameworks triggered by external stimuli. Acc Chem Res 50:778–786
158. Om Y, O'Keeffe M, Nw O, Hk C, Eddaoudi M, Kim J (2003) Reticular synthesis and the design of new materials. Nature 423:705–714. https://doi.org/10.1038/nature01650
159. Sumida K, Rogow DL, Mason JA, McDonald TM, Bloch ED, Herm ZR, Bae T-H, Long JR (2012) Carbon dioxide capture in metal–organic frameworks. Chem Rev 112:724–781. https://doi.org/10.1021/cr2003272
160. Mason JA, Sumida K, Herm ZR, Krishna R, Long JR (2011) Evaluating metal–organic frameworks for post-combustion carbon dioxide capture via temperature swing adsorption. Energy Environ Sci 4:3030–3040. https://doi.org/10.1039/C1EE01720A
161. Yang RT (2003) Adsorbents: fundamentals and applications. John Wiley & Sons, p 424. https://doi.org/10.1021/acs.accounts.6b00591
162. Keller JU, Staudt R (2005) Gas adsorption equilibria: experimental methods and adsorptive isotherms. Springer Science & Business Media, pp:1–422. https://doi.org/10.1007/b102056
163. Li J-R, Kuppler RJ, Zhou H-C (2009) Selective gas adsorption and separation in metal–organic frameworks. Chem Soc Rev 38:1477–1504. https://doi.org/10.1039/B802426J
164. Zhang Z, Zhao Y, Gong Q, Li Z, Li J (2013) MOFs for CO_2 capture and separation from flue gas mixtures: the effect of multifunctional sites on their adsorption capacity and selectivity. Chem Commun 49:653–661. https://doi.org/10.1039/C2CC35561B
165. Zhang S, Bai X, Zhao C et al (2021) Global CO_2 consumption by silicate rock chemical weathering: its past and future. Earths Future 9:e2020EF001938. https://doi.org/10.1029/2020EF001938
166. Shang K et al (2023) Study of urban heat island effect in Hangzhou metropolitan area based on SW-TES algorithm and image dichotomous model. SAGE Open 1-20:10–12. https://doi.org/10.1177/21582440231208851
167. Hu Z, Wang Y, Shah BB, Zhao D (2019) CO_2 capture in metal–organic framework adsorbents: an engineering perspective. Adv Sustain Syst 3:1800080. https://doi.org/10.1002/adsu.201800080
168. Milner PJ, Siegelman RL, Forse AC, Gonzalez MI, Runcevski TE, Martell JD, Reimer JA, Long JR (2017) A diaminopropane-appended metal–organic framework enabling efficient CO_2 capture from coal flue gas via a mixed adsorption mechanism. J Am Chem Soc 139:13541–13553. https://doi.org/10.1021/jacs.7b07612
169. Adhikari AK, Lin KS (2016) Improving CO_2 adsorption capacities and CO_2 /N_2 separation efficiencies of MOF-74 (Ni, Co) by doping palladium-containing activated carbon. Chem Eng J 284:1348–1360. https://doi.org/10.1016/j.cej.2015.09.086
170. Danaci D, Bui M, Dowell NM, Petit C (2020) Exploring the limits of adsorption-based CO_2 capture using MOFs with PVSA – from molecular design to process economics. Mol Syst Des Eng 5:212–231. https://doi.org/10.1039/C9ME00102F
171. Nordhaus WD (2007) A review of the stern review on the economics of climate change. J Econ Lit 45:686–702. https://doi.org/10.1257/jel.45.3.703
172. Hajilary N, Rezakazemi M (2018) CFD modeling of CO_2 capture by water-based nanofluids using hollow fiber membrane contactor. Int J Greenh Gas Con 77:88–95. https://doi.org/10.1016/j.ijggc.2018.08.002
173. Razavi SMR, Rezakazemi M, Albadarin AB, Shirazian S (2016) Simulation of CO_2 absorption by solution of ammonium ionic liquid in hollow-fiber contactors. Chem Eng Process 108:27–34. https://doi.org/10.1016/j.cep.2016.07.001
174. Soroush E, Mesbah M, Hajilary N, Rezakazemi M (2019) ANFIS modeling for prediction of CO_2 solubility in potassium and sodium based amino acid Salt solutions. J Environ Chem Eng 7:102925. https://doi.org/10.1016/j.jece.2019.102925
175. Walton KS, Millward AR, Dubbeldam D, Frost H, Low JJ, Yaghi OM, Snurr RQ (2008) Understanding inflections and steps in carbon dioxide adsorption isotherms in metal-organic frameworks. J Am Chem Soc 130:406–407. https://doi.org/10.1021/ja076595g
176. Samanta A, Zhao A, Shimizu GKH, Sarkar P, Gupta R (2012) Post-Combustion CO_2 capture using solid sorbents: a review. Ind Eng Chem Res 51:1438–1463. https://doi.org/10.1021/ie200686q
177. Li H, Eddaoudi M, O'Keeffe M, Yaghi OM (1999) Design and synthesis of an exceptionally stable and highly porous metal-organic framework. Nature 402:276–279. https://doi.org/10.1038/46248
178. Long JR, Yaghi OM (2009) The pervasive chemistry of metal–organic frameworks. Chem Soc Rev 38:1213–1214. https://doi.org/10.1039/B903811F
179. Mueller U, Schubert M, Teich F, Puetter H, Schierle-Arndt K, Pastre J (2006) Metal-organic frameworks-prospective industrial applications. J Mater Chem 16:626–636. https://doi.org/10.1039/B511962F
180. O'Keeffe M (2009) Design of MOFs and intellectual content in reticular chemistry: a personal view. Chem Soc Rev 38:1215–1217. https://doi.org/10.1039/B802802H
181. Koppens F, Folk J, Elzerman J, Hanson R, Van Beveren L, Vink I, Tranitz H, Wegscheider W, Kouwenhoven L, Vandersypen L (2005) Control and detection of singlet-triplet mixing in a random nuclear field. Science 309:1346–1350. https://doi.org/10.1126/science.1113719
182. Lawson S, Griffin C, Rapp K, Rownaghi AA, Rezaei F (2019) Amine-functionalized mil-101 monoliths for CO_2 removal from enclosed environments. Energy Fuel 33:2399–2407. https://doi.org/10.1021/ACS.ENERGYFUELS.8B04508
183. Chaemchuen S, Kabir NA, Zhou K, Verpoort F (2013) Metal–organic frameworks for upgrading biogas via CO_2 adsorption to biogas green energy. Chem Soc Rev 42:9304–9332. https://doi.org/10.1039/C3CS60244C
184. Tchalala M, Bhatt P, Chappanda K, Tavares S, Adil K, Belmabkhout Y, Shkurenko A, Cadiau A, Heymans N, De Weireld G (2019) Fluorinated MOF platform for selective removal and sensing of SO_2 from flue gas and air. Nat Commun 10:1328. https://doi.org/10.1038/s41467-019-09157-2
185. Clark CA, Heck KN, Powell CD, Wong MS (2019) Highly defective uio-66 materials for the adsorptive removal of perfluorooctanesulfonate. ACS Sustain Chem Eng 7:6619–6628. https://doi.org/10.1021/acssuschemeng.8b05572
186. Devic T, Serre C (2014) High valence 3p and transition metal based MOFs. Chem Soc Rev 43:6097–6115. https://doi.org/10.1039/C4CS00081A
187. Belmabkhout Y, Guillerm V, Eddaoudi M (2016) Low concentration CO_2 capture using physical adsorbents: are metal–organic frameworks becoming the new benchmark materials? Chem Eng J 296:386–397. https://doi.org/10.1016/j.cej.2016.03.124
188. Lin K-YA, Liu Y-T, Chen S-Y (2016) Adsorption of fluoride to UiO-66-NH_2 in water: stability, kinetic, isotherm and thermodynamic studies. J Colloid Interface Sci 461:79–87. https://doi.org/10.1016/j.jcis.2015.08.061
189. Ma M-Y, Yu L-Q, Wang S-W, Meng Y, Lv Y-K (2021) Hybrid ZIF-8-90 for selective solid-phase microextraction of exhaled breath from gastric cancer patients. Acs Appl Bio Mater 4:3608–3613. https://doi.org/10.1021/acsabm.1c00107
190. Rajagopalan AK, Rajendran A (2018) The effect of nitrogen adsorption on vacuum swing adsorption based post-combustion

CO_2 capture. Int J Greenh Gas Con 78:437–447. https://doi.org/10.1016/j.ijggc.2018.09.002
191. Maring BJ, Webley PA (2013) A new simplified pressure/vacuum swing adsorption model for rapid adsorbent screening for CO_2 capture applications. Int J Greenh Gas Con 15:16–31. https://doi.org/10.1016/j.ijggc.2013.01.009
192. Aaron D, Tsouris C (2005) Separation of CO_2 from flue gas: a review. Sep Sci Technol 40:321–348. https://doi.org/10.1081/SS-200042244
193. Yang Y, Guo Z, Chen X-H, Liu J (2019) A Ni_3O-cluster based porous MOF for catalytic conversion of CO_2 to cyclic carbonates. J Solid State Chem 276:190–193. https://doi.org/10.1016/J.JSSC.2019.05.010
194. Wu C, Irshad F, Luo M, Zhao Y, Ma X, Wang S (2019) Ruthenium complexes immobilized on an azolium based metal organic framework for highly efficient conversion of CO_2 into formic acid. ChemCatChem 11:1256–1263. https://doi.org/10.1002/cctc.201801701
195. Xiang W, Sun Z, Wu Y, He L-N, Liu C-j (2020) Enhanced cycloaddition of CO_2 to epichlorohydrin over zeolitic imidazolate frameworks with mixed linkers under solventless and co-catalyst-free condition. Catal Today 339:337–343. https://doi.org/10.1016/j.cattod.2019.01.050
196. Tian X, Rao F, Li C, Ge W, Lara NO, Song S, Xia L (2021) Solidification of municipal solid waste incineration fly ash and immobilization of heavy metals using waste glass in alkaline activation system. Chemosphere 283:131240. https://doi.org/10.1016/j.chemosphere.2021.131240
197. Gutberlet J (2015) Cooperative urban mining in Brazil: collective practices in selective household waste collection and recycling. Waste Manag 45:22–31. https://doi.org/10.1016/j.wasman.2015.06.023
198. Li H, Zhang N, Guo X-j, Dou M-y, Feng Q, Zou S, Huang F-c (2020) Summary of flue gas purification and treatment technology for domestic waste incineration. IOP Conference Series: Earth and Environmental Science 508:012016. https://doi.org/10.1088/1755-1315/508/1/012016
199. Khan NA, Hasan Z, Jhung SH (2013) Adsorptive removal of hazardous materials using metal-organic frameworks (MOFs): a review. J Hazard Mater 244-245:444–456. https://doi.org/10.1016/j.jhazmat.2012.11.011
200. Murdock CR, Hughes BC, Lu Z, Jenkins DM (2014) Cheminform abstract: Approaches for synthesizing breathing MOFs by exploiting dimensional rigidity. Coord Chem Rev 258–259:119–136. https://doi.org/10.1016/j.ccr.2013.09.006
201. Xiao T, Liu D (2019) The most advanced synthesis and a wide range of applications of MOF-74 and its derivatives. Microporous Mesoporous Mater 283:88–103. https://doi.org/10.1016/j.micromeso.2019.03.002
202. Czaja AU, Trukhan N, Müller U (2009) Enantioselective catalysis with homochiral metal-organic frameworks. Chem Soc Rev 38:1256–1284. https://doi.org/10.1039/B807083K
203. Jhung SH, Lee JH, Yoon JW, Serre C, Férey G, Chang JS (2007) Microwave synthesis of chromium terephthalate MIL-101 and its benzene sorption ability. Adv Mater 19:121–124. https://doi.org/10.1002/adma.200601604
204. Schüth F, Sing KSW, Weitkamp J (2008) Handbook of porous solids. Handbook of Porous Solids, p 3191. https://doi.org/10.1007/BF02492417
205. Yaghi OM (2002) Systematic design of pore size and functionality in isoreticular MOFs and their application in methane storage. Science 295:469–472. https://doi.org/10.1126/science.1067208
206. Sung H, Jhung N, Abedin K, Zubair H (2012) Analogous porous metal–organic frameworks: synthesis, stability and application in adsorption. Crystengcomm 14:7099–7109. https://doi.org/10.1039/C2CE25760B
207. Suh MP, Park HJ, Prasad TK, Lim DW (2009) Hydrogen storage in metal–organic frameworks. Chem Soc Rev 38:1294–1314. https://doi.org/10.1039/B802256A
208. Wu H, Gong Q, Olson DH, Li J (2012) Commensurate adsorption of hydrocarbons and alcohols in microporous metal organic frameworks. Chem Rev 112:836–868. https://doi.org/10.1021/cr200216x
209. Li J-R, Sculley J, Zhou H-C (2012) Metal–organic frameworks for separations. Chem Rev 112:869–932. https://doi.org/10.1021/cr200190s
210. Horcajada P, Gref R, Baati T, Allan PK, Maurin G, Couvreur P, Férey G, Morris RE, Serre C (2012) Metal–organic frameworks in biomedicine. Chem Rev 112:1232–1268. https://doi.org/10.1021/cr200256v
211. Lee J, Farha OK, Roberts JM, Scheidt KA, Nguyen ST, Hupp JT (2009) Metal-organic framework materials as catalysts. Chem Soc Rev 38:1450–1459. https://doi.org/10.1039/B807080F
212. Furukawa H, Ko N, Go YB, Aratani N, Choi SB, Choi E, Yazaydin AÖ, Snurr RQ, O'Keeffe M, Kim J, Yaghi OM (2010) Ultrahigh porosity in metal-organic frameworks. Science 329:424–428. https://doi.org/10.1126/science.1192160
213. Blanco-Brieva G, Campos-Martin JM, Al-Zahrani SM, Fierro JLG (2011) Effectiveness of metal–organic frameworks for removal of refractory organo-sulfur compound present in liquid fuels. Fuel 90:190–197. https://doi.org/10.1016/j.fuel.2010.08.008
214. Haque E, Lee JE, Jang IT, Hwang YK, Chang JS, Jegal J, Jhung SH (2010) Adsorptive removal of methyl orange from aqueous solution with metal-organic frameworks, porous chromium-benzenedicarboxylates. J Hazard Mater 181:535–542. https://doi.org/10.1016/j.jhazmat.2010.05.047
215. Khan NA, Jhung PSH (2012) Inside back cover: remarkable adsorption capacity of cucl2-loaded porous vanadium benzenedicarboxylate for benzothiophene. Angew Chem Int Edit 51:1281–1281. https://doi.org/10.1002/anie.201105113
216. Ahmed I, Khan NA, Hasan Z, Jhung SH (2013) Adsorptive denitrogenation of model fuels with porous metal-organic framework (MOF) MIL-101 impregnated with phosphotungstic acid: effect of acid site inclusion. J Hazard Mater 250-251:37–44. https://doi.org/10.1016/j.jhazmat.2013.01.024
217. Watanabe T, Sholl DS (2010) Molecular chemisorption on open metal sites in Cu(3)(benzenetricarboxylate)(2): a spatially periodic density functional theory study. J Chem Phys 133:094509. https://doi.org/10.1063/1.3479041
218. Petit C, Bandosz TJ (2012) Exploring the coordination chemistry of MOF–graphite oxide composites and their applications as adsorbents. Dalton T 41:4027–4035. https://doi.org/10.1039/c2dt12017h
219. Dathe H, Peringer E, Roberts VM, Jentys A, Lercher JA (2005) Metal organic frameworks based on Cu^{2+} and benzene-1,3,5-tricarboxylate as host for SO_2 trapping agents. Cr Chim 8:753–763. https://doi.org/10.1016/J.CRCI.2004.10.018
220. Yazaydın AOZR, Benin AI, Faheem SA, Jakubczak P, Snurr RQ (2009) Enhanced CO_2 adsorption in metal-organic frameworks via occupation of open-metal sites by coordinated water molecules. Chem Mater 21:1425–1430. https://doi.org/10.1021/CM900049X
221. Dietzel PDC, Besikiotis V, Blom R (2009) Application of metal-organic frameworks with coordinatively unsaturated metal sites in storage and separation of methane and carbon dioxide. J Mater Chem 19:7362–7370. https://doi.org/10.1039/B911242A
222. Caskey SR, Wong-Foy AG, Matzger AJ (2008) Dramatic tuning of carbon dioxide uptake via metal substitution in a coordination polymer with cylindrical pores. J Am Chem Soc 130:10870–10871. https://doi.org/10.1021/ja8036096

223. Cho HY, Yang DA, Kim J, Jeong SY, Ahn WS (2012) CO_2 adsorption and catalytic application of Co-MOF-74 synthesized by microwave heating. Catal Today 185:35–40. https://doi.org/10.1016/j.cattod.2011.08.019
224. Jung DW, Yang DA, Kim J, Kim J, Ahn WS (2010) Facile synthesis of MOF-177 by a sonochemical method using 1-methyl-2-pyrrolidinone as a solvent. Dalton T 39:2883–2887. https://doi.org/10.1039/B925088C
225. Yang DA, Cho HY, Kim J, Yang ST, Ahn WS (2012) CO_2 capture and conversion using Mg-MOF-74 prepared by a sonochemical method. Energy Environ Sci 5:6465–6473. https://doi.org/10.1039/C1EE02234B
226. Haque E, Khan NA, Kim CM, Jhung SH (2011) Syntheses of metal–organic frameworks and aluminophosphates under microwave heating: quantitative analysis of accelerations. Cryst Growth Des 11:4413–4421. https://doi.org/10.1021/cg200594e
227. An D, Chen HF, He RZ, Chen JQ (2024) MOF decorated boron nitride/natural rubber composites with heterostructure for thermal management application through dual passive cooling modes base on the improved thermal conductivity and water sorption-desorption process. Compos Sci Technol 248:110469. https://doi.org/10.1016/j.compscitech.2024.110469